

# Quantumness certification via non-demolition measurements

Paolo Solinas<sup>1</sup> and Stefano Gherardini<sup>2,3</sup>

<sup>1</sup>*Dipartimento di Fisica, Università di Genova, and INFN - Sezione di Genova, via Dodecaneso 33, I-16146, Genova, Italy.*

<sup>2</sup>*Istituto Nazionale di Ottica del Consiglio Nazionale delle Ricerche (CNR-INO), Largo Enrico Fermi 6, I-50125 Firenze, Italy.*

<sup>3</sup>*European Laboratory for Non-linear Spectroscopy, Università di Firenze, I-50019 Sesto Fiorentino, Italy.*

The fundamental question of when a static or dynamic system should be deemed intrinsically quantum remains a challenge to address in absolute terms. A rigorous criterion, however, can be established by focusing on the measurable or reconstructible features of the system. This determination transcends mere issues of a system's classical simulability or computational complexity. Instead, the critical requirement lies in the certification (ideally, in real-time) of the emergence and persistence of genuine quantum features, principally entanglement and quantum superposition. Quantum Non-Demolition Measurements (QNDM) serve as the appropriate instrument for this certification, both from a theoretical and experimental standpoint. In this review paper, we demonstrate, with accessible clarity, how the implementation of QNDM can be directly linked to a necessary and sufficient condition for the violation of macrorealism in finite-dimensional systems, establishing a conceptual parallel with Leggett-Garg inequalities. Using concrete examples that detail the detection of negative terms in the quasi-probability density function resulting from QNDM, we introduce the core concepts for certifying genuinely quantum features. As specific examples, we discuss an application where the quantum-to-classical transition due to the interaction with an environment can be tracked by QNDM. Moreover, we argue about the robustness of QNDM protocols in the presence of noise sources and their advantages with respect to the Leggett-Garg inequalities. Because of its straightforward implementation, the QNDM approach can be of direct relevance to both the foundations of quantum mechanics and quantum information theory, where a controlled generation and certification of genuinely quantum resources is a central concern.

## CONTENTS

|  |    |
|--|----|
| I. Introduction  | 2  |
| II. Motivation: Measuring work, heat, and internal energy variation at the quantum level | 3  |
| III. Quantum non-demolition measurement  | 4  |
| A. Application to driven systems: Measurement of quantum work                            | 7  |
| B. Non-demolition measurements for open quantum system                                   | 7  |
| IV. Macrorealism, quasi-probability distribution and Leggett-Garg inequalities           | 8  |
| A. Macrorealism  | 8  |
| B. Three-measurement scheme  | 9  |
| 1. Noninvasive measurability condition   | 9  |
| C. Necessary and sufficient condition for the violation of macrorealism                  | 10 |
| 1. Comparison with previous approaches   | 11 |
| D. Connection and comparison with Leggett-Garg inequalities                              | 12 |
| 1. Example   | 14 |
| V. Resources for realizing QNDM, and robustness against environmental noise              | 14 |
| VI. Tracking the quantum-to-classical transition   | 15 |
| VII. Conclusions   | 17 |
| A. What's Next?  | 17 |
| Acknowledgments  | 18 |
| References   | 18 |

## I. INTRODUCTION

Classical and quantum systems are intrinsically different in their properties and behaviours. Despite these evident differences, discriminating the quantum features of a system is extremely challenging because they are elusive and highly fragile, especially when put in contact with an external environment. Indeed, both the interaction with the environment and/or the measurement apparatus to extract information perturb the system and generally lead to the destruction of these features. Nevertheless, determining whether a system behaves in a classical or a quantum way is of paramount importance, both for the foundations of quantum mechanics and for the development of quantum technologies.

The main quantum features that cannot be developed by any classical system are entanglement and superposition (or interference). They are related to the concepts of nonlocality and macrorealism (MR), respectively. Traditionally, the criteria used to distinguish between classical and quantum systems and to identify the presence of such features are the famous Bell's inequalities [1–4] and the Leggett-Garg inequalities (LGIs) [5]. The former focuses on nonlocality and quantum correlations related to entanglement, while the latter concerns quantum superposition.

In this review, we focus on the macrorealistic properties of quantum systems, starting from the concept of macrorealism introduced by Leggett and Garg in 1985 [5]. According to the latter, a classical system must satisfy three main assumptions: 1) *Macrorealism per se* (MRps), which states that the system is at all times in one of the states available to it; 2) *Noninvasive Measurability* (NIM), which requires that it should be possible to determine the state of a system without disturbing its subsequent dynamics; and 3) *Induction*, added and clarified later [6], which asserts that future measurements cannot influence the present state. The conjunction of these assumptions can be tested experimentally. At a practical level, the NIM condition is difficult to implement. For this reason, it is often replaced by a statistical version called no-signalling in time (NSIT) [5–10]. More precisely, the NSIT conditions require that the unperturbed marginals of the probability distribution, defined at multiple times, can be recovered, where unperturbed means no changes in the state of the system are induced by quantum measurements.

By measuring time correlations between sequential measurements at two times, Leggett and Garg derived a set of inequalities [5], now known as LGIs, which are formally similar to Bell's inequalities. If these inequalities are not satisfied, then the system violates the macrorealism (MR) and therefore exhibits quantum features. LGIs, like Bell's inequalities, provide only a sufficient condition for the violation of MR. Indeed, there are situations in which a system violates MR, i.e., it has quantum properties, while still satisfying the LGIs.

Clearly, a protocol that provides both necessary and sufficient conditions for the violation of MR would be highly advantageous for identifying quantum features. Here, we review some recent works that address this gap by introducing an experimentally feasible and powerful protocol known as Quantum Non-Demolition Measurements (QNDM). This approach builds on measurement schemes proposed at the end of 1970s [11–15], which have been modified and adapted to extract information from sequential measurements [16–26], such that the assumptions defining the MR are fulfilled.

The key idea of QNDM is to store the information about a desired observable in the phase of a quantum detector that is coupled to the system. The coupling is designed so that it leaves the statistics of these observables unchanged. Then, after a sequence of system-detector interactions, the phase of the detector is measured, and from it one can reconstruct a quasi-probability density function of the measurement outcomes. The latter is not always positive, and it can be proven [26] that the presence of negative regions is unequivocally associated with the violation of MR. In other words, the quasi-probability density function has negative regions if and only if MRps is violated, and thus the presence of such regions provides both a necessary and sufficient condition for the violation of MR.

Comparable conditions have been presented in the literature [27–30], but in general they are weaker, namely are satisfied only for specific parameter choices, and are too difficult to verify in practice. In particular, in order to satisfy the conditions in Refs. [27–30], one has to solve a complex system of parametric equations, whose size grows with a power of the dimension of the measured quantum system. These limitations make the QNDM approach a privileged tool to study and identify the violation of MR and the presence of quantum behaviour.

The article is organized as follows. In Sec. II, we present a physical scenario in which we aim to extract information about work and internal energy variation of a quantum system. This is a prototypical example where the QNDM approach gives a consistent advantage over the standard projective measurements. It also provides the basis for Sec. III, where we introduce the QNDM protocol that is designed to preserve interference effects and quantum superposition. In Sec. IV, we discuss the relation between the QNDM protocol and LGIs, and we prove that it provides a necessary and sufficient condition for the violation of MR. Then, we discuss the resources needed to implement the QNDM compared to the LGIs (Sec. V) and an example where QNDM can be used to track the quantum-to-classical transition induced an external environment (Sec. VI), showing that the protocol is both robust against noise and efficient in terms of the resources required for its implementation. Finally, Sec. VII contains the conclusions and outlines future perspectives.

## II. MOTIVATION: MEASURING WORK, HEAT, AND INTERNAL ENERGY VARIATION AT THE QUANTUM LEVEL

The introduction of QNDM in recent literature [20–22, 26, 31] comes from a practical need: to give a clear and operational definition of physically relevant quantities such as work, heat, and internal energy variation at the quantum level.

Work, heat, and internal energy variation are cornerstone concepts in classical thermodynamics and mechanics. It is thus natural to ask how one can define or measure them when the dimension of the system under scrutiny decreases, and quantum effects become relevant. To illustrate the core problem but avoiding irrelevant complexity, we focus on the mechanical definition of internal energy variation and work. In other terms, we consider a system that is isolated from the environment, i.e., it does not dissipate energy in terms of heat, and that is driven by an external force that does work on the system. In this case, the work  $\mathcal{W}$  done by the external force is equal to the variation of the internal energy  $\Delta\mathcal{U}$ :  $\mathcal{W} = \Delta\mathcal{U}$ .

However, when we reach the quantum regime, we immediately face a problem whenever we need to measure and characterize the statistics of physical quantities intrinsically defined at two or multiple times. Indeed, in classical physics, we implicitly assume that we are able to measure these physical quantities without perturbing the system at any time. Instead, in quantum mechanics, the measurement procedure necessarily perturbs the system by inducing a collapse of its wave function [25].

This problem is well illustrated in the measurement of  $\mathcal{W}$  or  $\Delta\mathcal{U}$  in a quantum system. From a classical perspective, we can measure sequentially the energy of the system at the beginning  $\mathcal{E}_i$  and at the end  $\mathcal{E}_f$  of the driving protocol, and taking their difference:  $\mathcal{W} = \Delta\mathcal{U} = \mathcal{E}_f - \mathcal{E}_i$ . Here, all the physical quantities are well defined, and we thus have a clear theoretical definition that matches the measuring procedure.

In the quantum case, we suppose to know the time-dependent Hamiltonian  $\hat{H}(t)$  that defines the driving protocol. In particular, the time dependence of  $\hat{H}(t)$  is due to the presence of a classical external time-dependent force that exchanges energy with the quantum system, by doing work on it. The system evolves under  $\hat{H}(t)$  from time  $t = 0$  to time  $t = \mathcal{T}$ , undergoing a unitary transformation, which we denote as  $\hat{U}(\mathcal{T}) \equiv \hat{U}$ . The initial state of the system is supposed to be described by the density operator  $\hat{\rho}^0$ . As in the classical case, if the system is isolated, then the work is equal to the variation of the internal energy, but with a caveat. Indeed, the request is that the initial and final energies of the classical system are substituted by the statistical averages (expectation value) obtained from measuring the quantum system at times  $t = 0$  and  $t = \mathcal{T}$ :

$$\mathcal{W} = \Delta\mathcal{U} = \langle \hat{H}(\mathcal{T}) \rangle - \langle \hat{H}(0) \rangle = \text{Tr} \left[ \left( \hat{U}^\dagger \hat{H}(\mathcal{T}) \hat{U} - \hat{H}(0) \right) \hat{\rho}^0 \right]. \quad (1)$$

Looking at Eq. (1), one could define the work operator  $\hat{W} := \hat{U}^\dagger \hat{H}(\mathcal{T}) \hat{U} - \hat{H}(0)$  [32–34] that is Hermitian and allows us to interpret the average work as its trace over the initial density operator  $\hat{\rho}^0$ . However, the use of such an operator requires careful consideration as it hides a fundamental issue. Indeed, the average  $\mathcal{W}$  is related to two measurements performed sequentially at different times. This means that, even if  $\hat{W}$  is a Hermitian operator, it cannot be associated in general with a sequential measurement process since the latter is always local in time, at least in the usual projective measurement assumption [35].

Initially, this issue has been circumvented because the first studies considered initializing the quantum system under scrutiny in a thermal state built over the initial Hamiltonian  $\hat{H}(0)$ , for which sequential measurements suffice to determine two-time correlators. In such cases, one can adopt the so-called Two-Point Measurement (TPM) protocol [36–45]. This consists of measuring the system energy at the initial time  $t = 0$ , letting the system evolve under the external drive, and then measuring the energy at time  $t = \mathcal{T}$ . If we denote the eigenvalues and eigenvectors of  $\hat{H}(t)$  with  $\varepsilon_j(t)$  and  $|\varepsilon_j(t)\rangle$ , respectively, it can be shown [36, 37] that the statistics of the work (or internal energy variation) is given by the probability distribution

$$\mathcal{P}(W) = \sum_{i,j} \delta \left[ W - (\varepsilon_j(\mathcal{T}) - \varepsilon_i(0)) \right] P_i^{(0)} P_{i \rightarrow j}^{(\mathcal{T})}, \quad (2)$$

where  $P_i^{(0)} := \langle \varepsilon_i(0) | \hat{\rho}^0 | \varepsilon_i(0) \rangle$  is the probability to find the system initially in the state  $|\varepsilon_i(0)\rangle$ , and  $P_{i \rightarrow j}^{(\mathcal{T})} := |\langle \varepsilon_j(\mathcal{T}) | \hat{U} | \varepsilon_i(0) \rangle|^2$  is the probability for the occurrence of the transition from  $|\varepsilon_i(0)\rangle$  to  $|\varepsilon_j(\mathcal{T})\rangle$  due to the evolution  $\hat{U}$ . The average work provided by the TPM protocol can be obtained by the distribution (2) and reads

$$\mathcal{W} = \sum_{i,j} [\varepsilon_j(\mathcal{T}) - \varepsilon_i(0)] P_i^{(0)} P_{i \rightarrow j}^{(\mathcal{T})}. \quad (3)$$

Eqs. (2) and (3) have an immediate interpretation in simple statistical terms. The work done  $\varepsilon_j(\mathcal{T}) - \varepsilon_i(0)$  during the process is weighted by the probability to start from the state  $|\varepsilon_i(0)\rangle$  and to end in the state  $|\varepsilon_j(\mathcal{T})\rangle$  exactly as it happens in a classical statistical process.

Although its direct application, the first measurement of the TPM protocol causes a perturbation on the system, which leads to the collapse of the initial (at time  $t = 0$ ) system's wave-function. This ultimately entails a change in the dynamics and in the expected prediction [25]. To clarify this point, we consider the definition of the average work as given by Eq. (1) and show that, for a generic initial density operator  $\hat{\rho}^0$ , the TPM protocol cannot recover the full (unperturbed) expression of the average work.

Indeed, the right-hand side of Eq. (1) admits two contributions [19]: one related to the diagonal elements of  $\hat{\rho}^0$ , while the other depends on the corresponding off-diagonal elements. Formally, we have:

$$\mathcal{W} = \Delta\mathcal{W} = \sum_{i,j} [\varepsilon_j(\mathcal{T}) - \varepsilon_i(0)] P_i^{(0)} P_{i \rightarrow j}^{(\mathcal{T})} + \sum_{i \neq k,j} \varepsilon_j(\mathcal{T}) \rho_{i,k}^0 U_{k,j}^\dagger U_{j,i}, \quad (4)$$

where  $\sum_j P_{i \rightarrow j}^{(\mathcal{T})} = 1$  by construction,  $\rho_{i,k}^0 := \langle \varepsilon_i(0) | \hat{\rho}^0 | \varepsilon_k(0) \rangle$ ,  $U_{j,i} := \langle \varepsilon_j(\mathcal{T}) | \hat{U} | \varepsilon_i(0) \rangle$ ,  $U_{k,j}^\dagger := \langle \varepsilon_k(0) | \hat{U}^\dagger | \varepsilon_j(\mathcal{T}) \rangle$ . From this calculation, we evince that the difference between the unperturbed average work (4) and the average work returned by the TPM protocol (3) is in the contributions associated with the off-diagonal terms  $\rho_{i,k}^0$  of the initial density operator [19]. These contributions stem from the interference or coherent superposition of the eigenstates of the initial Hamiltonian  $\langle \hat{H}(0) \rangle$  [19–21].

This observation allows us to make a parallel with the famous two-slit experiment with quantum particles [46]. If both slits are open, we observe an interference pattern of the particle arriving at the screen. If one of the two slit is closed or we perform a measurement to establish through which slit the particle has passed, the interference pattern vanishes. In the present discussion, the initial projective measurement of  $\langle \hat{H}(0) \rangle$  leads to the collapse of the system's wave-function at  $t = 0$  and, as a consequence, forces the system into one of the eigenstates of  $\langle \hat{H}(0) \rangle$ . As in the two-slit experiment, the first measurement of the TPM protocol destroys the interference patterns and changes the subsequent dynamics of the system.

The challenge of measuring the variation of internal energy in a quantum system without destroying the quantum coherence and/or correlations, initially present in the system's state or generated during its dynamics, has been a subject of recent discussion in the literature. Specifically, pushed by no-go theorems [47, 48] that identify fundamental constraints on measuring physical quantities at two consecutive times, several approaches have been introduced. These include non-linear schemes using information about the initial system's state [49–53], initial-time measurements protocols [33, 54], procedures that implement weak measurements [55, 56], and quasi-probability approaches [22, 23, 48, 57–65]. Among the latter, we count Quantum Non-Demolition Measurements (QNDM) [12–15], which have been designed in order to acquire information about a quantum system at multiple times while preserving the full quantum dynamics of the system.

### III. QUANTUM NON-DEMOLITION MEASUREMENT

To better introduce the QNDM scheme, it is preferable to step back for the moment from the specific application discussed in the above section and consider a more general framework [26]. Below, we will show how these concepts directly apply to the measurement of the variation of internal energy.

Let us thus suppose we have a quantum system evolving under a unitary transformation in a time interval  $0 \leq t \leq \mathcal{T}$ . At times  $t_0 \leq t_1 = \mathcal{T}$ , we measure a generic observable  $\hat{A}$  (Hermitian operator). In order to realize QNDM, we consider an auxiliary quantum detector to store the desired information in the phase of the detector's state, which is eventually measured. This scheme allows us to preserve the quantum coherence in the initial density operator of the system, and obtain the quantum correlation function of observables measured at multiple times, without the result being perturbed by the interaction with the detector [20–23, 31].

Ideally, the sequential non-demolition measurements assume fast system-detector couplings so that, during the interaction with the detector, the system dynamics can be considered frozen. The main point in the QNDM approach is to choose a proper system-detector coupling. If we want to measure the observable  $\hat{A}$  we need to implement the unitary transformations  $\hat{u}_k = \exp\{i(\lambda_k/2)\hat{A} \otimes \hat{\rho}\}$  at any time  $t_k$  with  $k = 0, 1$  [19–21]. Here,  $\lambda$  is an effective coupling, and  $\hat{\rho}$  is an operator acting on the detector's degrees of freedom. The unitary transformations  $\hat{u}_k$  are taken in order to not induce any transition in the system state with respect to the basis that spectrally decomposes  $\hat{A}$ , whose statistics are thus preserved. Hence, the effect of the system-detector coupling is to make a phase accumulate in the detector state between the eigenstates  $\hat{\rho}$  of  $\hat{A}$ .

Between the couplings at times  $t_k$ , the system evolves freely from the detector. This means that there is no restriction on the system's time evolution that can also be driven by an external time-dependent field, which performs work on the system as in Sec. II. Such an evolution from time  $t_0$  to  $t_1$  is described by the unitary operator  $\hat{U}_1 \otimes \mathbb{1} = \hat{U}(t_1, t_0) \otimes \mathbb{1}$  so that the total unitary transformation acting on both the system and detector is  $\hat{U}_{tot} = \hat{u}_1(\hat{U}_1 \otimes \mathbb{1})\hat{u}_0$ . To keep the notation as simple as possible, we denote  $\hat{U}_i \equiv \hat{U}_i \otimes \mathbb{1}$  so that  $\hat{U}_{tot}$  reads

$$\hat{U}_{tot} = e^{i\frac{\lambda_1}{2}\hat{A} \otimes \hat{\rho}} \hat{U}_1 e^{i\frac{\lambda_0}{2}\hat{A} \otimes \hat{\rho}}. \quad (5)$$

This theoretical framework also accounts for sequential measurements of different operators. Indeed, considering that  $[\hat{U}_1, \hat{A}] \neq 0$  in the general case,  $\hat{U}_{tot}$  can be equivalently expressed as

$$\hat{U}_{tot} = \hat{U}_1 e^{i\frac{\lambda_1}{2}\hat{B} \otimes \hat{\rho}} e^{i\frac{\lambda_0}{2}\hat{A} \otimes \hat{\rho}}. \quad (6)$$

where  $\hat{B} := \hat{U}_1^\dagger \hat{A} \hat{U}_1$ .

To understand how the QNDM approach works, it is convenient to decompose the initial state of the system in the basis  $\{|i\rangle\}$  in which the observable  $\hat{A}$  is diagonal, i.e.,  $\hat{A}|i\rangle = a_i|i\rangle$  with  $a_i$  real numbers, so that  $|\psi_0\rangle = \sum_i \psi_i^0|i\rangle$ . At the same time, we must initialize the detector state in a coherent superposition of eigenstates of  $\hat{p}$ , so that it is taken equal to  $|\phi_0\rangle = \left(1/\sqrt{M}\right) \sum_p |p\rangle$ . This assures that, during the system-detector coupling, a phase is accumulated in the detector state between the eigenstates  $|p\rangle$ . Given the initial state  $|\psi_0\rangle|\phi_0\rangle$  and the unitary transformation  $\hat{U}_{tot}$ , the final system-detector state is (see Ref. [21, 24, 26] for analogous calculation)

$$|\Psi\rangle = \frac{1}{\sqrt{M}} \sum_p \sum_{i,j} e^{i\frac{\lambda p}{2}(a_j+a_i)} U_{1,ji} \psi_i^0 |j\rangle |p\rangle \quad (7)$$

where here  $U_{1,ji} := \langle j|\hat{U}_1|i\rangle$  and  $\lambda_0 = \lambda_1 = \lambda$ .

As the information on the evolution of the monitored system is extracted by measuring the phase accumulated in the detector state (experimentally, it can be done using an interferometric technique [62, 66, 67]), it is worth determining a formal expression for such a phase, whose meaning we are also going to discuss. Denoting with  $\hat{R} = |\Psi\rangle\langle\Psi|$ , the total density matrix after the evolution, we first trace out the system degrees of freedom to obtain the final density matrix  $\hat{r} = \text{Tr}_S [\hat{R}]$  of the detector. Second, we take the accumulated phase

$$\mathcal{G}_\lambda = \frac{\langle p|\hat{r}|-p\rangle}{\langle p|\hat{r}^0|-p\rangle}, \quad (8)$$

where  $\hat{r}^0 := |\phi_0\rangle\langle\phi_0|$ .

The function  $\mathcal{G}_\lambda$  defines the QNDM *quasi-characteristic function* associated with the correlation function of  $\hat{A}$  measured at  $t_0, t_1$ . It can be shown, indeed, that the derivatives of  $\mathcal{G}_\lambda$  with respect to  $\lambda$  at  $\lambda = 0$  are proportional to the moments of the distribution of the  $\hat{A}$  eigenvalues [20–23, 31]. Writing  $\mathcal{G}_\lambda$  as [19, 24, 25]

$$\mathcal{G}_\lambda = \text{Tr} \left[ e^{i\frac{\lambda}{2}\hat{A}} \hat{U}_1 e^{i\frac{\lambda}{2}\hat{A}} \hat{\rho}^0 e^{i\frac{\lambda}{2}\hat{A}} \hat{U}_1^\dagger e^{i\frac{\lambda}{2}\hat{A}} \right]. \quad (9)$$

and taking the first derivatives of  $\mathcal{G}_\lambda$  with respect to  $\lambda$  and setting  $\lambda = 0$ , we obtain the expectation value of the variation of  $\hat{A}$  within the time-interval  $[t_0, t_1]$  [19, 24]:

$$(-i) \frac{d\mathcal{G}_\lambda}{d\lambda} \Big|_{\lambda=0} = \text{Tr} \left[ \left( \hat{\rho}(t_1) - \hat{\rho}^0 \right) \hat{A} \right] = \langle \hat{A}(t_1) \rangle - \langle \hat{A}(t_0) \rangle = \langle \hat{A}^H(t_1) - \hat{A}(t_0) \rangle, \quad (10)$$

where  $\hat{\rho}(t_1) = \hat{U}_1 \hat{\rho}^0 \hat{U}_1^\dagger$ ,  $\langle \hat{A}(t_1) \rangle = \text{Tr}[\hat{A} \hat{\rho}(t_1)]$ , and  $\hat{A}^H(t_1) := \hat{U}_1^\dagger \hat{A} \hat{U}_1$  with the superscript  $H$  denoting the Heisenberg representation. Moreover, by direct calculation [24], it can be shown that the second derivative of  $\mathcal{G}_\lambda$  with respect to  $\lambda$ , computed at  $\lambda = 0$ , is proportional to  $\text{Tr} \left[ \left( \hat{A}^H(t_1) - \hat{A}(t_0) \right)^2 \hat{\rho}^0 \right]$ , which is the second moment of the variation of  $\hat{A}$ .

It should be stressed that these moments originated by the QNDM quasi-characteristic function  $\mathcal{G}_\lambda$  have a very specific time ordering. This is due to the fact that the operators  $\hat{A}^H(t)$  at different times  $t$  do not commute with each other. For example, in composing three operators using  $\hat{A}(t_0)$  and  $\hat{A}^H(t_1)$ , we have combinations such as  $\hat{A}^H(t_1) \hat{A}(t_0)^2$ ,  $\hat{A}^H(t_1)^2 \hat{A}(t_0)$ ,  $\hat{A}(t_0) \hat{A}^H(t_1) \hat{A}(t_0)$  and so on. The specific measurement procedure entails the time ordering; in general, different measurement protocol gives rise to different characteristic functions  $\mathcal{G}_\lambda$  that differ in the time ordering entering the statistical moments of  $\hat{A}^H(t_1) - \hat{A}(t_0)$ .

With these clarifications, given the final state in Eq. (7), we can calculate the QNDM quasi-characteristic function  $\mathcal{G}_\lambda$

$$\mathcal{G}_\lambda = \sum_{i,l,j} e^{i\lambda \left( a_j + \frac{a_i+a_l}{2} \right)} U_{1,ji} \rho_{ii}^0 U_{1,lj}^*, \quad (11)$$

that can be directly obtained experimentally as it is associated with the measurement of a phase, and, in this sense, it has a clear operational meaning.

Starting from the observation that  $\mathcal{G}_\lambda$  is a quasi-characteristic function, it is natural to ask what kind of probability distribution can be associated with it. As usual, the corresponding probability distribution is obtained by taking the inverse Fourier transform of  $\mathcal{G}_\lambda$ , i.e.,  $\mathcal{P}_{\text{QNDM}}(\Delta) = (2\pi)^{-1} \int \exp\{-i\lambda\Delta\} \mathcal{G}_\lambda d\lambda$ . It turns out that, in general,  $\mathcal{P}_{\text{QNDM}}(\Delta)$  is not positively defined and, therefore, is a quasi-probability density function. We must stress that  $\mathcal{P}_{\text{QNDM}}(\Delta)$  cannot be directly measured in an experiment, but reconstructed from the manipulation of the experimental data. This means that the negative regions of  $\mathcal{P}_{\text{QNDM}}(\Delta)$  have a physical interpretation, as discussed below, but are not associated with any physical observable.

To given an interpretation of the contributions in  $\mathcal{P}_{\text{QNDM}}(\Delta)$ , let us introduce the function

$$\Delta_{j,i,l} = a_j + \frac{a_i + a_l}{2}, \quad (12)$$

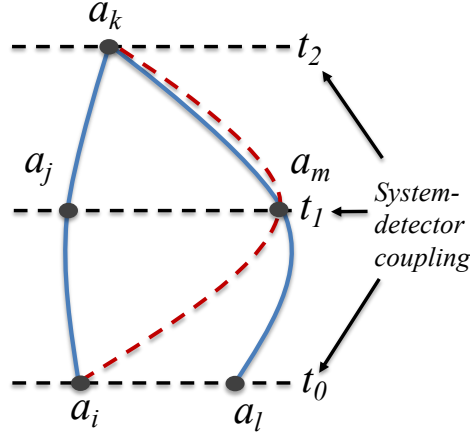


FIG. 1: A pictorial representation of the system's time evolution in terms of the outcomes from sequential measurements performed at three times  $(t_0, t_1, t_2)$ . In this picture, the trajectories developed by the measured system are ascribable to Feynman paths built over the measurement outcomes. The possible outcomes of the measurements are  $a_i$  and  $a_l$  at time  $t_0$ ,  $a_j$  and  $a_m$  at time  $t_1$ , and  $a_k$  at time  $t_2$ . The sequence of outcomes identifies the paths that the monitored system could follow during its time evolution. The red dashed curve represents a classical (macrorealistic) path where, at any time, we have a single outcome (e.g.,  $a_i \rightarrow a_m \rightarrow a_k$ ) so that the observable has a determinate outcome. The blue curves present quantum paths in which the system is in a superposition of states with different outcomes. In this case, the statistics of outcomes got from measuring  $\hat{A}$  change as the paths are no longer classical and violate the macrorealism requirement.

and the projectors  $\hat{\Pi}_k = |k\rangle\langle k|$  that obey the relations  $\hat{\Pi}_k^2 = \hat{\Pi}_k$ ,  $\sum_k \hat{\Pi}_k = \mathbb{1}$  and  $\hat{\Pi}_k \hat{\Pi}_j = \delta_{kj} \hat{\Pi}_k$ . With these notations, the QNDM quasi-probability density function can be formally written as

$$\mathcal{P}_{\text{QNDM}}(\Delta) = \sum_{i,l,j} P_{\text{QNDM}}(j,i,l) \delta[\Delta - \Delta_{j,i,l}], \quad (13)$$

where  $\delta[\cdot]$  denotes the Dirac's delta and

$$P_{\text{QNDM}}(j,i,l) = U_{1,ji} \rho_{ii}^0 U_{1,lj}^* = \text{Tr} [\hat{\Pi}_j \hat{U}_1 \hat{\Pi}_i \rho^0 \hat{\Pi}_l \hat{U}_1^\dagger]. \quad (14)$$

It is interesting to notice that  $P_{\text{QNDM}}(j,i,l)$  contains the Kirkwood-Dirac one [25, 63], which can be obtained by summing over the index  $l$  related to the quantum measurement with projectors  $\{\hat{\Pi}_l\}$ .

Eq. (13) allows us to have a direct interpretation of the contributions. The function  $P_{\text{QNDM}}(j,i,l)$  is the probability amplitude to arrive in the state  $|j\rangle$  following the superposition of paths  $i \rightarrow j$  and  $l \rightarrow j$ . A pictorial representation is presented in Fig. 1 where the measurement sequence is associated with a trajectory in the measurement outcomes space, e.g.,  $a_i \rightarrow a_j \rightarrow a_k$ .

Since  $P_{\text{QNDM}}(j,i,l)$  are probability amplitudes, they may take negative values from which the negativity of  $\mathcal{P}_{\text{QNDM}}(\Delta)$  comes. The  $P_{\text{QNDM}}(j,i,l)$  can be even complex numbers with imaginary parts, but the latter do not contribute to the non-positivity of the QNDM quasi-probability density function  $\mathcal{P}_{\text{QNDM}}(\Delta)$  for symmetry reasons, as it will be clarified below.

To understand the implications of the quasi-probability density function (13), let us separate its classical and quantum contributions. The classical contributions  $\mathcal{P}_{\text{cl}}(\Delta)$  of  $\mathcal{P}_{\text{QNDM}}(\Delta)$  are the ones in which, during the whole evolution, the system is always in an eigenstate of the measured observable (see Fig. 1 for a pictorial representation); as a consequence, they satisfy the MRps condition as presented in Sec. I. These are the contributions that can be assessed through the TPM protocol that relies on sequential projective measurements. The latter correspond to trajectories that can be associated with a positive (multitime) probability, and thus ascribable to classical evolutions in statistical mechanics. Formally, they are obtained from  $\mathcal{P}_{\text{QNDM}}(\Delta)$  when  $l = i$ , i.e.,

$$\mathcal{P}_{\text{cl}}(\Delta) = \sum_{i,j} P_{\text{QNDM}}(j,i,i) \delta[\Delta - \Delta_{j,i,i}], \quad (15)$$

where

$$P_{\text{QNDM}}(j,i,i) = U_{1,ji} \rho_{ii}^0 U_{1,ij}^* = P_i^{(0)} P_{i \rightarrow j}^{(1)}. \quad (16)$$

In Eq. (16),  $P_i^{(0)} = \rho_{ii}^0$  and  $P_{i \rightarrow j}^{(1)} = |U_{1,ji}|^2$  are the probabilities of finding the system initially in the state  $|i\rangle$  and then in the state  $|j\rangle$  after the transition  $|i\rangle \rightarrow |j\rangle$ , respectively. This proves that  $P_{\text{QNDM}}(j, i, i)$  is a positive probability.

On the other hand, the quantum contributions  $\mathcal{P}_q(\Delta)$  of  $\mathcal{P}_{\text{QNDM}}(\Delta)$  are the ones for which the system is in a superposition of the eigenstates of  $\hat{A}$  at any time  $t$  of the whole evolution (see Fig. 1) and, in the terminology used in Sec. I and Ref. [5], they are the ones that violate the MRPs assumption. In the easiest picture with two measurement times (e.g.,  $t_0, t_1$ ), the quantum contributions originate from considering  $l \neq i$ , which reflects the fact that the system is initially in a coherent superposition of the eigenstates  $|i\rangle$  and  $|l\rangle$  of  $\hat{A}$ . Hence, formally,

$$\mathcal{P}_q(\Delta) = \sum'_{i,l,j} P_{\text{QNDM}}(j, i, l) \delta[\Delta - \Delta_{j,i,l}], \quad (17)$$

where the notation  $\sum'$  denotes the sum over the indices  $i, l, j$  but neglecting the terms corresponding to  $l = i$ .

Let us now suppose that the measurement outcome  $a_i$  can be only  $\pm 1$ . The classical contributions in Eq. (15) are associated with  $\Delta_{j,i,i} = a_j + a_i$  that assume values 0 and  $\pm 2$ . On the contrary, the quantum contributions in Eq. (17) are associated with  $\Delta_{j,i,l}$  with  $l \neq i$  that also take values  $\pm 1$ . Therefore, in this sense, the quantum contributions of  $\mathcal{P}_{\text{QNDM}}(\Delta)$  are linked with sequences of measurement outcomes that are forbidden in classical transitions.

### A. Application to driven systems: Measurement of quantum work

The results in Sec. III can be applied to discuss how the QNDM approach can be exploited to measure the work in a closed quantum system. We only need to assume that at time  $t = 0$  the coupling between the system and the detector occurs with  $\hat{A} = \hat{H}(0)$ , at time  $\mathcal{T}$  it is with  $\hat{A} = \hat{H}(\mathcal{T})$  and, in the second coupling transformation, we flip the coupling sign  $\lambda \rightarrow -\lambda$  to store the variation, i.e., the difference, of the system energy in the detector state during the composite evolution.

Following the results in Eqs. (13), (15) and (17), the quasi-probability density function of work reads as

$$\mathcal{P}_{\text{QNDM}}(W) = \sum_{i,j} \delta \left[ W - (\varepsilon_j(\mathcal{T}) - \varepsilon_i(0)) \right] P_i^{(0)} P_{i \rightarrow j}^{(\mathcal{T})} + \sum_{i \neq l, j} \rho_{i,l}^0 U_{l,j}^\dagger U_{j,i} \delta [W - \Delta_{j,i,l}], \quad (18)$$

where here  $\Delta_{j,i,l} = \varepsilon_j(\mathcal{T}) - (\varepsilon_i(0) + \varepsilon_l(0))/2$ .

The average work can be calculated from the derivative of the corresponding quasi-characteristic function with respect to  $\lambda$ , as shown above, or directly from the distribution (18). It turns out to be equal to the expected average in Eq. (4), which is not recovered by the TPM scheme whenever the initial density operator  $\hat{\rho}^0$  is not diagonal along the eigenbasis of  $\hat{H}(0)$  [47, 48].

Importantly, we have observed that every time the TPM protocol fails to reproduce the unperturbed value  $\text{Tr}[\hat{W}\hat{\rho}^0]$  for the average work  $\mathcal{W}$ , then the QNDM quasi-probability density function of the work exhibits at least a negative region. The reason for this behaviour has a broader explanation that we can identify in the violation of macrorealism, as we will discuss in the following. Specifically, for a work distribution, these negative regions are associated with non-classical energy exchanges. For example, consider a two-level system with bare Hamiltonian  $\hat{H} = (\hbar\omega/2)\hat{\sigma}_z$ , where  $\hat{\sigma}_z$  is the Pauli matrix along the  $z$ -axis. The system is driven by a cyclic transformation. This means that the energy spectrum is the same at the beginning and at the end of the system time evolution, i.e., the energies  $\varepsilon_j(\mathcal{T})$  and  $\varepsilon_j(0)$  ( $j = 1, 2$ ) take the same values  $\pm\hbar\omega/2$ . The TPM scheme — providing the classical contribution to  $\mathcal{P}_{\text{QNDM}}(W)$  — allows only for energy exchanges equal to 0 and  $\pm\hbar\omega$ . On the contrary, due to the presence of quantum coherence in the initial density operators  $\hat{\rho}^0$ , the work distribution develops quantum contributions, and the support of  $\mathcal{P}_{\text{QNDM}}(W)$  comprises the work realizations  $\pm\hbar\omega/2, 0$ , and  $\pm\hbar\omega$ . The ‘fractional’ energy exchanges  $\pm\hbar\omega/2$  are not allowed by any classical and statistical interpretation, and cannot be recovered by the TPM scheme.

We point out that the experimental protocol consists in measuring experimentally the quasi-characteristic function  $\mathcal{G}_\lambda$  such that  $\mathcal{P}_{\text{QNDM}}(W)$  is reconstructed from the analysis of the experimental data. In addition, we observe that the first and second moments of the QNDM work quasi-probability density function have a clear physical interpretation, extending the validity of these concepts from classical thermodynamics. However, the structure (in particular, the time-ordering) of the higher statistical moments may not be physically motivated. The latter, indeed, are ultimately determined and cannot be separated by the measurement procedure.

### B. Non-demolition measurements for open quantum system

In this section, we briefly discuss the application of the QNDM protocol to open quantum systems [68]. We will then make use of these concepts in Sec. VI, where they will be contextualized for the tracking of the quantum-to-classical transition.

In order to keep the presentation affordable, we are going to argue the main ideas and advantages of applying QNDM to monitor the dissipated heat in coherently-driven and open (due to system-environment interactions) dynamics.

The dissipated heat is a process function, and thus depends on the full time evolution of the system. For example, a quantum system starting and ending in the ground state does not change its overall internal energy. However, due to the interaction with the external environment, the system can produce a possibly arbitrary amount of heat during the open dynamics, through a sequence of excitations and relaxations. The only way to keep track of the dissipated heat is by constantly monitoring the system dynamics.

When it comes to the dissipated heat at the quantum level, a standard approach to this problem [69] is to perform sequential measurements of the *environment degrees of freedom*, in order to evaluate the energy dissipated into the environment, which is identified as heat. However, this approach may be both conceptually and practically unfeasible.

First, in many applications, a nanoscale system couples with an environment that has to be considered macroscopic, namely possessing a virtually infinite number of degrees of freedom and an essentially infinite heat capacitance. This entails a common approximation (Born's approximation) [68, 70] done in dealing with open quantum system dynamics, i.e., to assume that the state of the environment does not change because of the interaction with the nanoscale system. As a result, from a practical point of view, one would need to detect any absorbed/emitted energy quantum from the environment, or at least to statistically sample a large portion of the environmental degrees of freedom.

Second, an environment with a small number of degrees of freedom changes its state because of the absorption or emission of an energy quantum, and it behaves quantum mechanically. These energy exchanges would lead to a non-equilibrium environment (e.g., an environment without a definite temperature), so it must be treated as an additional evolving quantum system. In addition, a measurement on it induces a wave-function collapse, destroying (partially or totally) its properties.

These conditions are so restrictive that only a few proposals have been able to meet all the requirements to fulfil them. For example, in Ref. [71–76], the use of an auxiliary system is proposed to collect the dissipated energy, under the assumption that the auxiliary system has a quantized spectrum and at the same time enough degrees of freedom to act as an intermediate, effective environment. However, despite these rare situations, it seems questionable whether the proposal to measure the environmental energy can always be exploited efficiently.

The QNDM approach can overcome these drawbacks for monitoring the heat, because it is designed to extract information from the *system degrees of freedom*, without inducing any perturbation on the dynamics (no-signalling in time condition). The important requirement to use the QNDM approach to monitor the heat over time is that the time-scales of the external drive (performing work on the system) and the environment are separated [20]. Under this assumption, we can exploit [19] the result stating that time-changes of the system Hamiltonian are associated with work, while time-changes in the system density operator are associated with dissipated heat [77]. Hence, performing fast sequential measurements, the monitoring of the system's internal energy changes leads to reconstructing energy dissipation in terms of heat. Then, over a longer time scale, the effects due to the external drive in terms of work can also be included, with the constraint of respecting the first law of thermodynamics [20].

## IV. MACROREALISM, QUASI-PROBABILITY DISTRIBUTION AND LEGGETT-GARG INEQUALITIES

### A. Macrorealism

The original definition of Macrorealism per se (MRps) [5], which was prone to different interpretations, has been recently clarified [78, 79]. Specifically, once the observable to measure is identified, the assumption of MRps is satisfied if *quantum superpositions are not allowed, at any time, within the Hilbert space spanned by the eigenbasis of the observable or by a statistical mixture of them* [79]. The assumption of MRps is thus satisfied if there cannot be *coherent superpositions* and the state of the system is always diagonal in the basis that diagonalizes the measurement observable [79, 80].

The Noninvasive Measurability (NIM) assumption, entering the Macrorealism (MR), is equally difficult to formalize. For this reason, it is usually flanked by the No-Signalling In Time (NSIT) conditions [6, 7] that are a less strong version of NIM. This allows us to relate the NIM with the possibility of attaining the marginal probability of single events from the joint probability of a sequence of them, without the results being perturbed by any intermediate measurement [6]. As an example, if  $p(s(t_0), s(t_1), s(t_2))$  is a generic joint probability at the three times  $(t_0, t_1, t_2)$ , then the NSIT condition for the outcome  $s(t_2)$  ensures that  $\sum_{s(t_0), s(t_1)} p(s(t_0), s(t_1), s(t_2)) = P(s(t_2))$ , where  $P(s(t_2))$  is the probability to measure  $s(t_2)$  in correspondence of the system state at time  $t_2$  where the measurement is performed. This assures that no previous measurements in the sequence have statistically affected the system state. Throughout the remaining part of the paper, the symbol  $P$  will denote both probabilities at single times, given by Born's rule, and probabilities at multiple times respecting the theory of classical probability (in particular, the Kolmogorov axioms).

Below, we will show that the QNDM quasiprobabilities always satisfy the NSIT assumption; hence, the violation of MR can be reduced only to the violation of the MRps, for which both a necessary and sufficient condition can be given. Formally, ensuring the validity of such a necessary and sufficient condition certifies the presence and/or development of quantum features in the system state under scrutiny.

## B. Three-measurement scheme

The simplest and most used version of the Leggett-Garg inequalities (LGIs) [5] is based on a three measurement scheme [6, 10]. To discuss the relations between the QNDM protocol, LGIs, and the macrorealism violation, we extend the protocol discussed in Sec. III to the three-measurement scheme depicted in Fig. 1. For technical details, the reader can refer to Ref. [26].

Let us thus consider a system that evolves under a unitary transformation in the time interval  $0 \leq t \leq \mathcal{T}$ , and the system observable  $\hat{A}$  is measured sequentially at times  $t_0 \leq t_1 \leq t_2 = \mathcal{T}$ . As above, the measurements of  $\hat{A}$  are performed by coupling the system with a detector that interacts through the operator  $\hat{u}$ . The system time evolution in between the measurements is governed by the unitary operators  $\hat{U}_k \equiv \hat{U}(t_k, t_{k-1}) \otimes \mathbb{1}$  with  $k = 1, 2$ . Hence, overall, the time evolution operator  $\hat{U}_{tot}$  for the system-detector within the interval  $[t_0, t_2]$  read as

$$\hat{U}_{tot} = \hat{u}\hat{U}_2\hat{u}\hat{U}_1\hat{u} = e^{i\frac{\lambda}{2}\hat{A}\otimes\hat{p}}\hat{U}_2e^{i\frac{\lambda}{2}\hat{A}\otimes\hat{p}}\hat{U}_1e^{i\frac{\lambda}{2}\hat{A}\otimes\hat{p}}. \quad (19)$$

Assuming same initial states, notations and definitions as in Sec. III, the QNDM quasi-characteristic function is [26]

$$\mathcal{G}_\lambda = \sum_{i,l,j,m,k} e^{i\lambda\left(a_k + \frac{a_j + a_m + a_i + a_l}{2}\right)} U_{2,kj} U_{1,ji} \rho_{il}^0 U_{1,lm}^* U_{2,mk}^*, \quad (20)$$

where

$$\Delta_{k,j,m,i,l} := a_k + \frac{a_j + a_m + a_i + a_l}{2} \quad (21)$$

denotes the spectrum of measurement outcomes at times  $t_0, t_1, t_2$ .

By direct calculation of the inverse Fourier transform of the QNDM quasi-characteristic function (20), we obtain the quasi-probability density function  $\mathcal{P}_{\text{QNDM}}(\Delta)$  that is formally equal to

$$\mathcal{P}_{\text{QNDM}}(\Delta) = \sum_{i,l,j,m,k} P_{\text{QNDM}}(k, j, m, i, l) \delta[\Delta - \Delta_{k,j,m,i,l}]. \quad (22)$$

In Eq. (22),

$$P_{\text{QNDM}}(k, j, m, i, l) = U_{2,kj} U_{1,ji} \rho_{il}^0 U_{1,lm}^* U_{2,mk}^* = \text{Tr} \left[ \hat{\Pi}_k \hat{U}_2 \hat{\Pi}_j \hat{U}_1 \hat{\Pi}_i \hat{\rho}^0 \hat{\Pi}_l \hat{U}_1^\dagger \hat{\Pi}_m \hat{U}_2^\dagger \right]. \quad (23)$$

are the probability amplitudes for the system to arrive in the state  $|k\rangle$  following the superposition of paths  $i \rightarrow j \rightarrow k$  and  $l \rightarrow m \rightarrow k$  (see Fig. 1).

Again, we can separate the classical  $\mathcal{P}_{cl}(\Delta)$  from the quantum  $\mathcal{P}_q(\Delta)$  contributions of  $\mathcal{P}_{\text{QNDM}}(\Delta)$ . The first ones are obtained when  $m = j$  and  $l = i$ ,

$$\mathcal{P}_{cl}(\Delta) = \sum_{i,j,k} P_{\text{QNDM}}(k, j, j, i, i) \delta[\Delta - \Delta_{k,j,j,i,i}], \quad (24)$$

and they are given by positive probabilities since  $P_{\text{QNDM}}(k, j, j, i, i) = P_i^{(0)} P_{i \rightarrow j}^{(1)} P_{j \rightarrow k}^{(2)}$  where  $P_i^{(0)} = \rho_{ii}^0$  and  $\{P_{i \rightarrow j}^{(1)} = |U_{1,ji}|^2, P_{j \rightarrow k}^{(2)} = |U_{2,kj}|^2\}$  are the probabilities that the system is initially in the state  $|i\rangle$  and then makes a transition from state  $|i\rangle$  to  $|j\rangle$  and from  $|j\rangle$  to  $|k\rangle$ , respectively.

The quantum contributions  $\mathcal{P}_q(\Delta)$  of  $\mathcal{P}_{\text{QNDM}}(\Delta)$ , instead, are present when  $m \neq j$  or  $l \neq i$ , and thus they are associated with the coherent superposition of paths or trajectories in the space identified by the sequence of measurement outcomes [19, 26]. They formally read as

$$\mathcal{P}_q(\Delta) = \sum'_{i,l,j,m,k} P_{\text{QNDM}}(k, j, m, i, l) \delta[\Delta - \Delta_{k,j,m,i,l}], \quad (25)$$

where the sum  $\sum'$  includes contributions with  $(l = i, m \neq j)$ ,  $(m = j, l \neq i)$  and  $(m \neq j, l \neq i)$ . These are the conditions under which the system is in a superposition of the  $\hat{A}$  eigenstates, at least one of the measurements in the sequence.

### 1. Noninvasive measurability condition

It can be checked that  $\mathcal{P}_{\text{QNDM}}(\Delta)$  in Eq. (22) satisfies the NSIT condition. That is, the marginals of  $\mathcal{P}_{\text{QNDM}}(\Delta)$ , over all the measurement outcomes but the ones at a single time, return the ‘unperturbed’ probability to measure the observable  $\hat{A}$  [?] given by the Born’s rule, without any intermediate measurement of the sequence affects the result.

To see this in the three-measurement scheme, the probability  $P(a_k)$  of measuring the outcome  $a_k$  at time  $t_2$  is computed by summing the QNDM quasi-probability  $P_{\text{QNDM}}(k, j, m, i, l)$  over all the intermediate outcomes  $a_i, a_l, a_j, a_m$ . Using the properties of the projectors, i.e.,  $\hat{\Pi}_k^2 = \hat{\Pi}_k$ ,  $\sum_k \hat{\Pi}_k = \mathbb{1}$  and  $\hat{\Pi}_k \hat{\Pi}_j = \delta_{kj} \hat{\Pi}_k$ , we find:

$$\begin{aligned} P(a_k) &= \sum_{i,l,j,m} P_{ND}(k, j, m, i, l) = \sum_{i,l,j,m} \text{Tr} \left[ \hat{\Pi}_k \hat{U}_2 \hat{\Pi}_j \hat{U}_1 \hat{\Pi}_i \hat{\rho}^0 \hat{\Pi}_l \hat{U}_1^\dagger \hat{\Pi}_m \hat{U}_2^\dagger \right] = \\ &= \text{Tr} \left[ \hat{\Pi}_k \hat{U} \hat{\rho}^0 \hat{U}^\dagger \right] = \text{Tr} \left[ \hat{\Pi}_k \hat{\rho}(t_2) \right], \end{aligned} \quad (26)$$

where here  $\hat{U} = \hat{U}_2 \hat{U}_1$  and  $\hat{\rho}(t_2) = \hat{U} \hat{\rho}^0 \hat{U}^\dagger$ . Therefore,  $P(a_k)$  is the probability to record the measurement outcome  $a_k$  at time  $t_2$  as given by Born's rule [6].

We also compute the single-time probabilities  $P(a_i)$ ,  $P(a_l)$  for the initial measurement at time  $t_0 = 0$ :

$$\begin{aligned} P(a_i) &= \frac{1}{2} \sum_{l,j,m,k} \left\{ P_{ND}(k, j, m, i, l) + P_{ND}(k, j, m, l, i) \right\} = \\ &= \frac{1}{2} \sum_{l,j,m,k} \left\{ \text{Tr} \left[ \hat{\Pi}_k \hat{U}_2 \hat{\Pi}_j \hat{U}_1 \hat{\Pi}_i \hat{\rho}^0 \hat{\Pi}_l \hat{U}_1^\dagger \hat{\Pi}_m \hat{U}_2^\dagger \right] + \text{Tr} \left[ \hat{\Pi}_k \hat{U}_2 \hat{\Pi}_j \hat{U}_1 \hat{\Pi}_l \hat{\rho}^0 \hat{\Pi}_i \hat{U}_1^\dagger \hat{\Pi}_m \hat{U}_2^\dagger \right] \right\} = \\ &= \text{Tr} \left[ \hat{\Pi}_i \hat{\rho}^0 \right]. \end{aligned} \quad (27)$$

and

$$P(a_l) = \frac{1}{2} \sum_{i,j,m,k} \left\{ P_{ND}(k, j, m, i, l) + P_{ND}(k, j, m, l, i) \right\} = \text{Tr} \left[ \hat{\Pi}_l \hat{\rho}^0 \right]; \quad (28)$$

both these probabilities satisfy Born's rule, as well as  $P(a_k)$ .

Moreover, for the measurement at time  $t_1$ , there are two possible realizations over the indices  $j$  and  $m$ , so that

$$P(a_j) = \frac{1}{2} \sum_{i,l,m,k} \left\{ P_{ND}(k, j, m, i, l) + P_{ND}(k, m, j, i, l) \right\} = \text{Tr} \left[ \hat{\Pi}_j \hat{U}_1 \hat{\rho}^0 \hat{U}_1^\dagger \right] = \text{Tr} \left[ \hat{\Pi}_j \hat{\rho}(t_1) \right] \quad (29)$$

that is to the probability of recording the outcome  $a_j$  after the system has evolved to the state  $\hat{\rho}(t_1) = \hat{U}_1 \hat{\rho}^0 \hat{U}_1^\dagger$ , without the initial measurement at time  $t = 0$  has affected the system state.

Finally, if we sum the QNDM quasi-probabilities  $P_{\text{QNDM}}(k, j, m, i, l)$  over three indices return the Kirkwood-Dirac quasi-probabilities at two-times [25, 48, 63], apart from the 3-tuples  $(j, m, k)$  and  $(i, l, k)$  that give rise to a single-time probability. By definition, Kirkwood-Dirac quasi-probabilities respect the NSIT assumption.

### C. Necessary and sufficient condition for the violation of macrorealism

It can be proved [26] that *a system is in a coherent superposition of the measured observable's eigenstates if and only if the QNDM quasi-probability density function  $\mathcal{P}_{\text{QNDM}}(\Delta)$  exhibits negativity, i.e., it has negative contributions*. The fact that the measured system is in a superposition state violates the MRps and, consequently, the MR. Therefore, the statement above can also be formulated as: *the MR is violated if and only if  $\mathcal{P}_{\text{QNDM}}(\Delta)$  has negative contributions*.

This result is based on the following three main properties of the QNDM protocol. First, the QNDM quasi-probability density function  $\mathcal{P}_{\text{QNDM}}(\Delta)$  comprises only real numbers. Second,  $\mathcal{P}_{\text{QNDM}}(\Delta)$  is normalized to 1, and this normalization comes uniquely from the classical contribution  $\mathcal{P}_{cl}(\Delta)$ . The first and second properties imply that the terms entering the quantum contribution  $\mathcal{P}_q(\Delta)$  of  $\mathcal{P}_{\text{QNDM}}(\Delta)$  cancel out each other, such that some of them must be negative. The last property, which directly links with the violation of the macrorealism, is that the negativity of  $\mathcal{P}_{\text{QNDM}}(\Delta)$  appears whenever the system is in a superposition of the measurement observable's eigenstates.

Let us argue about the meaning of the necessary and sufficient conditions for the violation of MR. From the one side, since the negativity of  $\mathcal{P}_{\text{QNDM}}(\Delta)$  derives from contributions in  $\mathcal{P}_q(\Delta)$ , a *necessary condition* for the negativity of  $\mathcal{P}_{\text{QNDM}}(\Delta)$  is that the system is in a coherent superposition of the observable  $\hat{A}$ 's eigenstates at times  $t_0$  or  $t_1$  or  $t_2$ . On the other hand, the fact that the system is in a coherent superposition state is also a *sufficient condition* for the negativity of  $\mathcal{P}_{\text{QNDM}}(\Delta)$ . This is because the negativity of  $\mathcal{P}_{\text{QNDM}}(\Delta)$  can derive *only* from  $\mathcal{P}_q(\Delta)$ , whose integral over all values of  $\Delta$  is equal to zero:  $\int d\Delta \mathcal{P}_q(\Delta) = 0$ . This constraint imposes that, whenever  $\mathcal{P}_q(\Delta) \neq 0$ ,  $\mathcal{P}_{\text{QNDM}}(\Delta)$  must contain negative real terms.

Two observations are now in order. First, by construction,  $\mathcal{P}_q(\Delta)$  comprises real numbers that are the real parts of  $P_{\text{QNDM}}(k, j, m, i, l)$ , complex numbers. This means that the sum of  $P_{\text{QNDM}}(k, j, m, i, l)$  could vanish even if the system is a coherent superposition of  $\hat{A}$ 's eigenstates, when the quasiprobabilities  $P_{\text{QNDM}}(k, j, m, i, l)$  are purely imaginary. To avoid this, it is sufficient to run the measurement protocol two more times, by performing the additional unitary transformation  $\hat{U}_\chi := \exp\{i\chi\hat{A}\}$  on the system — with  $\chi$  a given angle — first at time  $t_0$  and then at time  $t_1$  in the second run. The transformation  $\hat{U}_\chi$  just adds a phase in the system state and does not induce transitions between the eigenstates of the observable  $\hat{A}$ . Therefore, it does not change the fact that the system is in a superposition state and thus that it may satisfy the assumption of MRps. A proper choice of  $\chi$  (even sampled by a probability distribution could be a good option) ensures that every pure imaginary amplitude encoded in  $P_{\text{QNDM}}(k, j, m, i, l)$  acquires a real part, resulting in a  $\mathcal{P}_q(\Delta) \neq 0$ .

In addition, for practical implementations, the whole procedure for quantumness certification becomes more *robust* if the second and third measurements at times  $t_1$  and  $t_2$  are made over the measurement observable with slightly shifted coupling parameters:  $\lambda \rightarrow \lambda' = \lambda + \delta$  and  $\lambda \rightarrow \lambda'' = \lambda + \delta'$ . These measurements are realized by applying the unitary transformation  $\hat{u}_\delta := e^{i\frac{\lambda'}{2}\hat{A}\otimes\hat{p}}$  and  $\hat{u}_{\delta'} := e^{i\frac{\lambda''}{2}\hat{A}\otimes\hat{p}}$  to the system-detector. The advantages of applying  $\hat{u}_\delta, \hat{u}_{\delta'}$  are to split the support of  $\mathcal{P}_{\text{QNDM}}(\Delta)$  in  $\Delta$  and to remove the degeneracy among the different paths that are associated with the same value of  $\Delta_{k,j,m,i,l}$ . For example, for  $i = j, l = m$  and  $i \neq l$ , the system is in a coherent superposition of states and  $\Delta = a_k$ . However, the same value of  $\Delta$  is also associated to the classical path with  $i = l$  and  $j = m$ . This fact could happen for binary observables (see also below) when  $(a_i = a_j = 1, a_m = a_l = -1)$  or  $(a_i = a_j = -1, a_m = a_l = 1)$ . But if we split the support of  $\mathcal{P}_{\text{QNDM}}(\Delta)$ , we can guarantee that both classical and quantum contributions are present in  $\Delta$ .

Overall, the procedure for operationally certifying a violation of MR is given by the following three runs of experiments:

$$\begin{aligned} (1) \quad \hat{U}_{1ot} &= e^{i\frac{\lambda''}{2}\hat{A}\otimes\hat{p}}\hat{U}_2 e^{i\frac{\lambda'}{2}\hat{A}\otimes\hat{p}}\hat{U}_1 e^{i\frac{\lambda}{2}\hat{A}\otimes\hat{p}} \\ (2) \quad \hat{U}_{1ot} &= e^{i\frac{\lambda''}{2}\hat{A}\otimes\hat{p}}\hat{U}_2 e^{i\frac{\lambda'}{2}\hat{A}\otimes\hat{p}}\hat{U}_1 e^{i\frac{\lambda}{2}\hat{A}\otimes\hat{p}} e^{i\chi\hat{A}\otimes\mathbb{1}} \\ (3) \quad \hat{U}_{1ot} &= e^{i\frac{\lambda''}{2}\hat{A}\otimes\hat{p}}\hat{U}_2 e^{i\frac{\lambda'}{2}\hat{A}\otimes\hat{p}} e^{i\chi\hat{A}\otimes\mathbb{1}}\hat{U}_1 e^{i\frac{\lambda}{2}\hat{A}\otimes\hat{p}}. \end{aligned}$$

If none of the resulting QNDM quasi-probability density functions  $\mathcal{P}_{\text{QNDM}}(\Delta)$  show negative regions, then MR is fulfilled, meaning that the system under scrutiny can be considered as classical according to the measurement observable  $\hat{A}$ . This means that the system has definite properties at all times, and it satisfies the MR conditions.

### 1. Comparison with previous approaches

In the literature, there are already some papers that address the existence of a necessary and sufficient condition for the violation of MR. Among them, it is worth mentioning the ones by Clemente and Kofler [27, 28] and by Halliwell [29, 30]. In particular, in Ref. [30], the Author makes a quite accurate review of theoretical approaches that aim to identify MR violations.

In Ref. [30], Halliwell distinguishes between two approaches for identifying a violation of MR, denoted respectively as MR-weak and MR-strong, which are derived from two versions of NIM: the “weak” or “piecewise” NIM (NIM-pw) and the “strong” or “sequential” one (NIM-seq). NIM-pw is inherently satisfied in a Leggett–Garg measurement scheme, while NIM-seq is operationally replaced by the NSIT conditions, which are statistically equivalent.

As discussed in Ref. [30], the MR-weak approach is not always able to detect quantum coherences (or interferences) that are present in the initial state of the system or generated dynamically. By contrast, the MR-strong approach provides a much stronger framework for identifying MR violations, although it is not guaranteed that NIM-seq is satisfied for any choice of parameters entering the initial state and the measurement observable. In this regard, from [30] we quote the sentence “it is, therefore, necessary to adjust the initial state and measurement times (and perhaps other parameters too) to ensure that the NSIT conditions are satisfied”, whose analogue with the same meaning can be found in the example and summary table of Ref. [27]. This is because, for any given combination of initial state, system dynamics, and measurements, ensuring that the NSIT conditions are valid at all times (three times in our case study) requires solving a system of many parametric equations [27]. The size of this system grows with the dimension of the system under consideration. Moreover, it is not guaranteed that the system of equations always admits solutions that confirm or exclude violations of MR [30].

For quantum systems with many degrees of freedom or highly correlated dynamics, it may be difficult or even impossible to verify the validity of the NSIT conditions. Indeed, it is unknown whether there exists a set of parameters (initial state, evolution, and measurements) that leads to the violation of at least one NSIT condition in the presence of quantum coherence and/or correlations in the system state [27, 30]. This fact is clearly stated in Ref. [27], where it is written: “While our results suggest that an experimental demonstration of nonclassicalities requires either very precise measurements or a complex time evolution, a general proof of this trade-off (in terms of experimental control parameters) is still missing.”

Given this context, the QNDM approach is instead a viable, operational protocol to certify MR. Such an approach falls within the category of NIM-seq, as it satisfies all NSIT conditions by construction. Moreover, the QNDM protocol is designed to

identify a violation of MRps, independently of the initial state, measurement observables, or time evolution of the system. These violations are certified by examining a single quantity: the negativity of the QNDM quasi-probability density function. In addition, the QNDM approach has already found successful application in many experimental scenarios [22, 23, 81–84], as it only requires coupling the measured system with a detector via a phase operator that has broad experimental applicability. In particular, in Refs. [22, 23], QNDM have been employed to monitor the loss of coherence due to environmental effects in commercial IBM quantum processors. These tests have shown that a QNDM protocol can be realized even in a setting hardly affected by noise.

Similar ideas of using an additional quantum system to reconstruct features of a quantum system has been proposed also in the field of full-counting statistics [85–87], where the statistics of electrons flowing through a wire is measured. While it was known that the approach of full-counting statistics can lead to a quasi-probability distribution [55, 87–90], implications in terms of macrorealism violation and the connection of the latter to the negativity of the quasi-probability distribution have not been fully understood. However, it is worth mentioning that the results derived using full-counting statistics led to several implementations in condensed matter and electronic circuits [91–93], thus bringing advancement in such fields.

#### D. Connection and comparison with Leggett-Garg inequalities

In this section, we compare the procedure for detecting MR violations via the QNDM protocol with the usual tool employed so far to identify the violation of MRps, i.e., the Leggett-Garg inequalities. The LGIs are usually formulated for binary observables [5, 6, 8, 10], namely for observables that can have two outcomes. Hence, we now assume that the eigenvalues of the observable  $\hat{A}$  are  $a_i = \pm 1$  for any time  $t_i$ . LGIs are built using quantum correlators at two times, say  $t_i$  and  $t_j$ , which are defined as [6, 8, 10]

$$C_{ij} = \frac{1}{2} \text{Tr} \left[ \left( \hat{A}^H(t_i) \hat{A}^H(t_j) + \hat{A}^H(t_j) \hat{A}^H(t_i) \right) \hat{\rho}^0 \right] \quad (30)$$

with  $\hat{A}^H(t_i) = \hat{U}^\dagger(t_i, 0) \hat{A} \hat{U}(t_i, 0)$  represented in Heisenberg picture. The expression of  $C_{ij}$  can be rewritten as

$$C_{ij} = \sum_{i,j,k} a_i a_j P(a_k, a_j, a_i) = \sum_{i,j,k} a_i a_j P_i^{(0)} P_{i \rightarrow j}^{(1)} P_{j \rightarrow k}^{(2)} = \sum_{i,j,k} a_i a_j P_{\text{QNDM}}(k, j, j, i, i), \quad (31)$$

where  $P(a_k, a_j, a_i) = P_i^{(0)} P_{i \rightarrow j}^{(1)} P_{j \rightarrow k}^{(2)} = P_{\text{QNDM}}(k, j, j, i, i)$  is the joint probability to record the measurement outcomes  $a_k, a_j, a_i$  at three consecutive times using a sequential scheme of projective measurements. Following Ref. [10], we introduce the Leggett-Garg (LG) parameter

$$K := C_{01} + C_{12} - C_{02} \quad (32)$$

that reads as  $K = 1 - 4 [P(1, -1, 1) + P(-1, 1, -1)]$  and obeys the LGI  $-3 \leq K \leq 1$  if the system under consideration is classical and fulfils all MR assumptions. This means that, if the  $-3 \leq K \leq 1$  is not satisfied, then at least one condition of MR is violated. However, the opposite is not guaranteed because there are cases where the MR is violated, but the value of  $K$  is still included in the range  $-3 \leq K \leq 1$ .

Starting from the QNDM quasi-probability density function (22), the correlators  $C_{ij}$  can be equivalently expressed as [6, 26]

$$C_{ij} = \sum_{i,j} a_i a_j P_{\text{QNDM}}(j, i), \quad (33)$$

where

$$\begin{aligned} P_{\text{QNDM}}(j, i) = & \sum_{l,m,k} [P_{\text{QNDM}}(k, j, m, i, l) + P_{\text{QNDM}}(k, m, j, i, l) + \\ & + P_{\text{QNDM}}(k, j, m, l, i) + P_{\text{QNDM}}(k, m, j, l, i)] \end{aligned} \quad (34)$$

are Kirkwood-Dirac quasi-probabilities [25, 48, 63], as commented in Sec. IV B 1. From Eq. (33), we can evince that the correlators entering the LGI  $-3 \leq K \leq 1$  are functions of QNDM quasiprobabilities at three times, whose distribution thus has full information about the LG parameter  $K$ . Accordingly, using the QNDM quasi-probability density function, one can directly single out the value of  $K$  and understand whether the LGI is violated.

We now report the expression of the LG parameter  $K$  as a function of the QNDM quasi-probabilities at three times; the derivation of this result is in Ref. [26]. Since we are working with binary variables, each of them can take two values:  $a_i$  and  $-a_i$ .

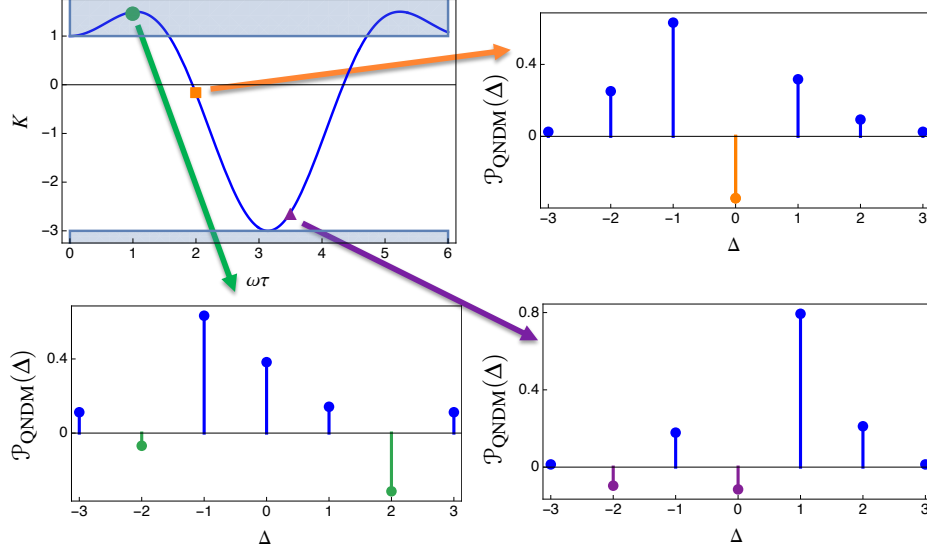


FIG. 2: Comparison between the prediction of the LGI and QNDM approach. In the top-left panel, we plot the LG parameter  $K$  as a function of  $\omega\tau$ . The shaded regions are the ones for which the LGI is violated. The other panels show the quasi-probability distribution  $\mathcal{P}_{\text{QNDM}}(\Delta)$  evaluated at three different values of  $\omega\tau$ . The distribution  $\mathcal{P}_{\text{QNDM}}(\Delta)$  always shows negative regions, while only for the green circle point the LGI is violated.

For simplicity, we refer to them with the indices  $i$  and  $\bar{i}$ ; for example,  $P_{\text{QNDM}}(\bar{k}, j, m, i, \bar{i})$  stands for  $P_{\text{QNDM}}(-a_k, a_j, a_m, a_i, -a_i)$ . Using Eq. (33), the LG parameter  $K$  of Eq. (32) reads as

$$K = \frac{1}{4} \sum_{i,l,j,m,k} f(k, j, m, i, l) P_{\text{QNDM}}(k, j, m, i, l) \quad (35)$$

with  $f(k, j, m, i, l) = (a_i + a_l)(a_j + a_m) + a_k(a_j + a_m - a_i - a_l)$ . It is convenient to separate  $K$  in its classical and quantum contributions:  $K = K_{cl} + K_{q,1} + K_{q,2}$ . The classical contribution is obtained when  $(m = j, l = i)$ , while the quantum ones  $K_{q,1}$  and  $K_{q,2}$  correspond to  $(m = j, l = \bar{i} \neq i)$  and  $(m = \bar{j} \neq j, l = i)$ , respectively. It can be shown [26] that  $K_{cl}$  satisfies the LGI, i.e.,  $-3 \leq K_{cl} \leq 1$ , and that  $K_{q,1} = 0$ . Therefore, when present, the violation of the LGI is due to the second quantum contribution  $K_{q,2}$  of  $K$ , which is equal to

$$K_{q,2} = -4 \sum_k \text{Re} [P_{\text{QNDM}}(k, j, \bar{j}, k, k)]. \quad (36)$$

From this analysis, we can learn that the contributions with  $m = \bar{j} \neq j$  and  $l = i$ , entailed by the superposition between eigenstates of  $\hat{A}$ , are the ones responsible for the violation of the LGI. This implies, in turn, that whenever the MRps is violated but the LGI is satisfied, we are dealing with a combination of initial state, system dynamics, and measurement observable such that  $K_{q,2}$  vanishes. In such a case, the total quantum contribution  $K_q$  vanishes as well,  $K_q = 0$ , with the result that  $K = K_{cl}$ , confirming that the violation of the LGI is only a sufficient condition for identifying MR violations. Indeed, there could be trajectories in which  $l \neq i$ , meaning that the system is initially in a superposition of  $\hat{A}$ 's eigenstates that naturally violates the MRps. These trajectories cannot be identified by LGI since  $K_{q,1} = 0$ . On the contrary, if we use  $\mathcal{P}_{\text{QNDM}}(\Delta)$ , the terms  $P_{\text{QNDM}}(k, j, j, i, \bar{i})$  in (22) always contribute to negative regions of the distribution, whose presence is both a sufficient and necessary condition for the violation of the MRps and thus of MR.

Overall, detecting violations of MR using the framework of NSIT conditions provides a significantly robust criterion [27, 28]. However, for complex quantum systems with many degrees of freedom or strongly correlated dynamics, verifying whether the NSIT conditions are fulfilled can be very challenging. Many solutions proposed so far in the literature [27–30] to evaluate MR do not work in general, except for a specific choice of parameters, initial state, and measurement times. These constraints are not present in the QNDM approach, which can therefore represent an operational protocol for quantumness certification, at the price, however, of using an auxiliary system acting as a detector.

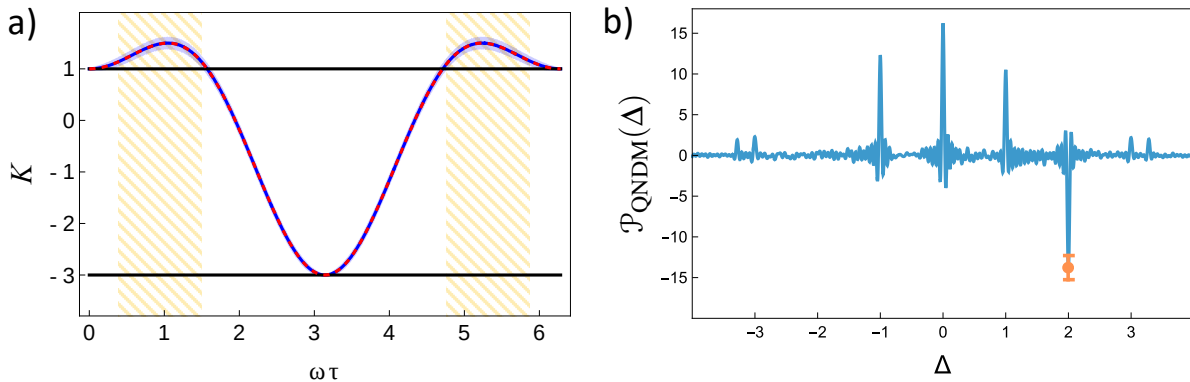


FIG. 3: a) Simulation results for the computation of the LG parameter  $K = C_{01} + C_{12} - C_{02}$  in a scenario where the measurement statistical uncertainty is present, with  $N_{\text{shots}} = 10^4$ . The solid blue line represents the simulated average curve (obtained over  $N_{\text{shots}}$  repetitions), while the dashed red line corresponds to the theoretical prediction as given in the example at the end of Sec. IV D. The blue-shaded region originates from the statistical uncertainty, while the yellow-shaded regions highlight the range of  $\omega\tau$  where, considering statistical errors, a violation of the LGI is confidently detected. b) Plot of the quasi-probability density functions  $\mathcal{P}_{\text{QNDM}}(\Delta)$  for  $\delta\lambda = 1$  and  $N_{\text{shots}} = 10^2$ . These curves are obtained by taking the inverse Fourier transform of the simulated data for  $\omega\tau = 1.5$ , and the orange error bars represent the statistical uncertainty. Notice that, in order to extract single probability values from  $\mathcal{P}_{\text{QNDM}}(\Delta)$ , we must integrate it over a fixed interval of  $\Delta$ . The negative region in  $\mathcal{P}_{\text{QNDM}}(\Delta)$  is visible for any value of  $\omega\tau$ . These panels are adapted from figures in Ref. [94].

### 1. Example

In order to clarify how the QNDM approach works and performs against the traditional LGIs, we report a specific example (present also in Refs. [6, 26]). We consider a two-level quantum system that is initialized in the state  $|\psi_0\rangle = (|0\rangle + i|1\rangle)/\sqrt{2}$  where  $|0\rangle$  and  $|1\rangle$  are the eigenstates of the Pauli operator  $\hat{\sigma}_z$ . The dynamics is generated by the Hamiltonian  $\hat{H} = \omega\hat{\sigma}_x/2$ , and we measure the operator  $\hat{A} = \hat{\sigma}_z$  at times  $t_0 = 0$ ,  $t_1 = \tau$  and  $t_2 = 2\tau$ .

The correlators  $C_{ij}$  and the corresponding LG parameter  $K$  can be calculated analytically, such that  $K = 2\cos(\omega\tau) - \cos(2\omega\tau)$ . As discussed above, any value of  $K$  outside the range  $[-3, 1]$  implies the violation of at least one MR condition; instead, it is not guaranteed that the MR holds if  $-3 \leq K \leq 1$ .

The numerical results for the example are shown in Fig. 2. The top-left panel shows the value of  $K$  as a function of  $\omega\tau$  with the shaded regions representing the situations in which the LGI is violated. The colored shapes (dot, square, triangle) give the value of  $K$  for three specific values of  $\omega\tau$ . The other panels of Fig. 2 depict the QNDM quasi-probability distribution associated with each colored shape. In correspondence of the green circle, the LGI is violated and the corresponding QNDM distribution  $\mathcal{P}_{\text{QNDM}}(\Delta)$  has negative regions. However, for the other two colored shapes (the orange square and the purple circle), a more interesting fact occurs: while the LGI is satisfied,  $\mathcal{P}_{\text{QNDM}}(\Delta)$  presents negative regions, and it allows us to identify quantum features of the system even when the LGI fails. From the analytical expression of  $K$ , the violation of the LGI occurs for  $0 \leq \omega\tau \leq \pi/2$  and  $3\pi/2 \leq \omega\tau \leq 2\pi$ . Hence, in this example, the LGI correctly identifies the violation of MRps in only half of the cases, while the QNDM protocol always succeeds.

## V. RESOURCES FOR REALIZING QNDM, AND ROBUSTNESS AGAINST ENVIRONMENTAL NOISE

As discussed in Secs. IV C and IV D, the QNDM approach allows for the identification of the violation of MR even when the LGI fails. It is thus natural to ask how many resources one needs to realize a sequence of non-demolition measurements, and compare them to the resources required to reconstruct the LGI. Here, we refer to the protocols discussed in Sec. IV D, including the example in IV D 1, by performing a detailed comparison of the implementation costs following Ref. [94].

For this purpose, we fix the number of repetitions  $N_{\text{shots}}$  of the protocols, and we multiply  $N_{\text{shots}}$  by the resources for the single repetition. To determine the three correlators entering the definition of the LG parameter  $K = C_{01} + C_{12} - C_{02}$ , we have to run the experiment three times. Therefore, to reconstruct  $K$ , the same procedure has to be repeated  $N_{\text{LG}} = 3N_{\text{shots}}$  times. Instead, concerning non-demolition measurements, each sequence of them is associated with a specific value of  $\lambda$ . For example, if we take  $0 \leq \lambda \leq 100$  with discretization  $\delta\lambda = 0.1$ , this accounts for a total of  $N_\lambda = 10^3$  experiments. Considering that for each value of  $\lambda$ , we need to measure both the real and imaginary parts of the quasi-characteristic function  $\mathcal{G}_\lambda$ , the total number of protocol repetitions is  $N_{\text{QNDM}} = 2N_\lambda N_{\text{shots}}$ .

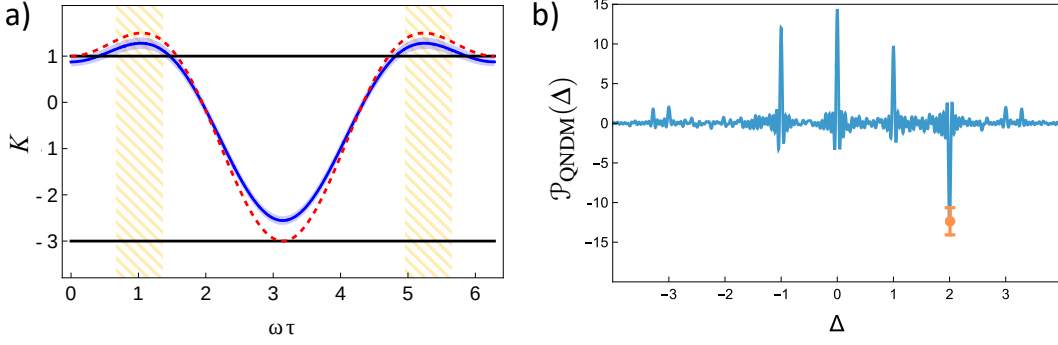


FIG. 4: a) Simulation results for the computation of the LG parameter  $K = C_{01} + C_{12} - C_{02}$  in the presence of both environmental noise and quantum gate errors for  $N_{\text{shots}} = 10^4$ . b) Plot of  $\mathcal{P}_{\text{QNDM}}(\Delta)$  for  $\delta\lambda = 1$  and  $N_{\text{shots}} = 10^2$ . In all panels, the notation and parameters are as in Fig. 3. These panels are adapted from figures in Ref. [94].

Now, let us focus on how statistical uncertainty, due to a finite number of experimental repetitions, affects the accuracy with which a MR violation can be identified for both the LG and QNDM protocols. In Fig. 3 panel a), we show the LG parameter  $K$  obtained by computing the correlators  $C_{01}, C_{12}, C_{02}$  in simulation with  $N_{\text{shots}} = 10^4$ , while in panel b) we plot the QNDM quasi-probability density function  $\mathcal{P}_{\text{QNDM}}(\Delta)$ , using  $N_{\text{shots}} = 10^2$  experimental repetitions with  $\delta\lambda = 1$  (thus,  $N_\lambda = 10^2$ ). This means that, to run the experiments, we need similar resources:  $N_{\text{LG}} = 3 \cdot 10^4$  and  $N_{\text{QNDM}} = 2 \cdot 10^4$ .

In panel a) of Fig. 3, the blue shaded regions are delineated by the variance associated with the statistical uncertainty of measurements, while the yellow-shaded regions represent the interval of  $\omega\tau$  where we are “statistically certain” to violate the LGI. The dashed red curve represents the ideal value of  $K$  (i.e., with no statistical uncertainty), while the solid blue curve is the mean value of  $K$  averaged over the experimental repetitions. In the ideal case, violations of the LGI occur in the ranges  $0 \leq \omega\tau \leq \pi/2$  and  $3\pi/2 \leq \omega\tau \leq 2\pi$ , covering 50% of the total  $\omega\tau$  range. The presence of measurement statistical uncertainty significantly reduces the confidence interval for the LGI’s violation to 38% of the total  $\omega\tau$  range [94].

Panel b) of Fig. 3 shows the QNDM quasi-probability density function obtained with  $\omega\tau = 1.5$ . According to the QNDM protocol, we need to take into account many values of  $\mathcal{G}_\lambda$ ; in this case, we take  $0 \leq \lambda \leq 100$  with discretization  $\delta\lambda = 1$ . As we can see from the figure, the negative region of  $\mathcal{P}_{\text{QNDM}}(\Delta)$  around  $\Delta = 2$  is clearly visible, identifying the presence of quantum effects. It turns out that the negative region is visible for any value of  $\omega\tau$ , albeit in the presence of a measurement statistical uncertainty. With these parameters, the QNDM protocol identifies the violation of MR for any  $\omega\tau$ , requiring a comparable amount of resources to those needed to compute the LG parameter  $K$ . We conclude that, with the same amount of resources, the QNDM always identifies the violation of MR while the LGI fails in about 60% of the cases.

In realistic experiments, we have to take into account also the environmental noise due to the interaction with the external environment, and errors due to the imprecise implementation of the unitary transformations. To see how these noise/error sources can affect the computation of both  $K = C_{01} + C_{12} - C_{02}$  and the QNDM quasi-probability density function, we run simulations on a 5-qubit IBM quantum processor using the simulator FakeBogotaV2 [95]. The obtained results are presented in Fig. 4.

Panel a) of Fig. 4 refers to  $N_{\text{shots}} = 10^4$  repetitions, for a total of  $N_{\text{LG}} = 3 \cdot 10^4$  repetitions. From the figure, we can see that the regions where the LGI is violated are further shrunk to 24% of the total  $\omega\tau$  range, respectively. These results show that the use of the LGI as a witness of an MR violation may be problematic in the presence of environmental noise and gate/control errors.

Panel b) of Fig. 4 displays the QNDM quasi-probability density function obtained with  $N_{\text{shots}} = 10^2$  and  $\delta\lambda = 1$  for a total of  $N_{\text{QNDM}} = 2 \cdot 10^4$  repetitions. Despite a quite low level of resources and the presence of environmental noise, the negative region of  $\mathcal{P}_{\text{QNDM}}(\Delta)$  is still clearly visible. Therefore, in this case, the advantage of using QNDM is even more pronounced since, with a fully comparable amount of resources, they allow for identifying the violation of the MR, while the LGI fails roughly in 75% of cases.

## VI. TRACKING THE QUANTUM-TO-CLASSICAL TRANSITION

A relevant application for the use of the QNDM approach is the tracking of the quantum-to-classical transition due to the interaction with the environment. The quantum-to-classical transition can be identified by looking at the reduction of the negative regions of  $\mathcal{P}_{\text{QNDM}}(\Delta)$  [22, 23].

As a prototypical example, let us consider a two-level system  $S$  subject to an external drive, and interacting with an external engineered environment  $E$ . The engineered environment allows us to control the coupling strength between the system and the environment. The evolution of the system and the detector is as described above: a sequence of non-demolition measurements at discrete times  $t_i$  via a fast, transient coupling with a detector  $D$  interspersed with the system unitary transformations.

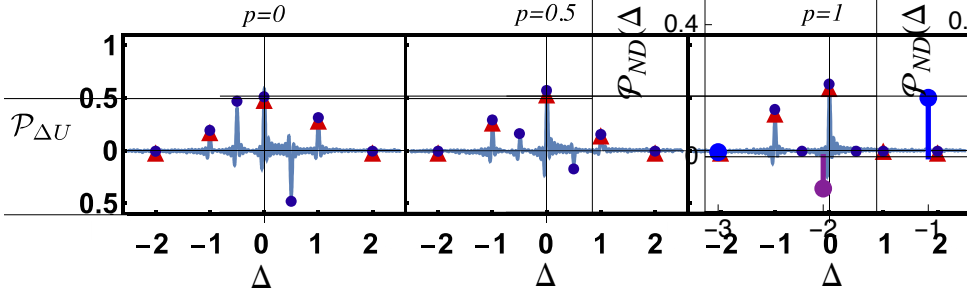


FIG. 5: QNDM quasi-probability density function  $\mathcal{P}_{\Delta U}$  of the internal energy variation  $\Delta U$  for a qubit interacting with an environment inducing relaxation. The relaxation strength is parameterized by  $p$  that goes from  $p = 0$  (no dissipation) to  $p = 1$  (full relaxation process).  $\mathcal{P}_{\Delta U}$  is calculated using experimental data obtained from the IBM quantum processor IBMQ-VIGO [95]. The blue dots and the red triangles are the predictions of the QNDM and TPM schemes, respectively. In the experiments, we set  $\theta = 0.7$ ,  $\phi = 1.2$  for the initial state, and  $\alpha = 1$ ,  $\beta = 0.5$  for the system dynamics. The figure is taken from Ref. [22].

For the sake of clarity, here the physical problem is measuring the work, the internal energy variation, and the heat, as in Sec. III A. But, since we are dealing with an open quantum system, the internal energy variation comprises both the work done on the system and the heat dissipated into the environment [22, 23]. To avoid any superfluous complexity, we will focus only on the internal energy variation, which is obtained by measuring the energy of the system at the start and the end of the thermodynamic transformation [22, 23].

The two-level system evolves under the unitary evolution  $\hat{U}_S = \hat{U}_z \hat{U}_x$ , where  $\hat{U}_z = \exp(-i\beta \hat{\sigma}_z / \hbar)$  and  $\hat{U}_x = \exp(-i\alpha \hat{\sigma}_x / \hbar)$ , with  $\hat{\sigma}_i$  ( $i = x, y, z$ ) denoting the Pauli operators. This system evolution is generated by the time-dependent Hamiltonian  $\hat{H}_S(t)$ , where  $\hat{H}_S = \varepsilon \hat{\sigma}_x / 2$  for  $t_0 \leq t < t_1$  and  $\hat{H}_S = \varepsilon \hat{\sigma}_z / 2$  for  $t_1 < t \leq \mathcal{T}$ . The initial state of the system is  $|\psi_0\rangle = \cos(\frac{\theta}{2})|0\rangle_S + \sin(\frac{\theta}{2})e^{i\phi}|1\rangle_S$ .

The detector  $D$  is represented by an additional two-level system whose dynamics is supposed to be frozen during the full evolution of the measured system  $S$ . The initial state of the detector is  $(|0\rangle_D + |1\rangle_D) / \sqrt{2}$ .

The Hamiltonian that governs the coupling between the system and the detector is  $\hat{H}_{SD}(t) = f(t)\hat{H}_S(t) \otimes \hat{H}_D$ , which is operated at times  $t_0 = 0$  and  $\mathcal{T}$ . The system-detector coupling at these two times suffices to encode information about the internal energy variation of the system in the phase of the detector state. The time-dependence  $f(t)$  in the coupling is chosen in order to implement the unitary transformations  $\hat{u}_0 = \exp\{-(i\lambda/\hbar) \hat{\sigma}_x \otimes \hat{H}_D\}$  and  $\hat{u}_{\mathcal{T}} = \exp\{-(i\lambda/\hbar) \hat{\sigma}_z \otimes \hat{H}_D\}$ . We assume that the system-detector coupling occurs over times much smaller than  $\varepsilon^{-1}$ , which is the timescale of the system dynamics.

In addition, we take into account an engineered open dynamics modelled by an amplitude-damping channel [96, 97]. This means that the environment induces the relaxation of the system from the excited to the ground states with probability  $p$ , and the relaxation process is associated with a dissipated energy. The parameter  $p$  determines the strength of the dissipation process, and it ranges from  $p = 0$  (no dissipation) to  $p = 1$  (complete relaxation to the ground state).

To realize the effects of the amplitude-damping channel on the system, we use an additional two-level system, such that the effective system-environment dynamics is described by the transformation

$$\begin{aligned} |00\rangle_{SE} &\rightarrow |00\rangle_{SE} \\ |10\rangle_{SE} &\rightarrow \sqrt{1-p}|10\rangle_{SE} + \sqrt{p}|01\rangle_{SE}, \end{aligned} \quad (37)$$

where the first and the second qubits represent the system and the environment, respectively. The transformation in Eq. (37) models the emission of an energy quantum with probability  $p$ , whereby we suppose that the environment can only induce relaxation, and not excitation in the system. The relaxation occurs in the basis that diagonalizes  $\hat{H}_S(t)$ , namely in the basis of  $\hat{\sigma}_x$  for  $0 \leq t \leq t_1$  and in the basis of  $\hat{\sigma}_z$  for  $t_1 \leq t \leq \mathcal{T}$ . For simplicity, we denote with  $\hat{R}_x$  and  $\hat{R}_z$  the operators (acting on the system and environment degrees of freedom) that implement the transformation (37). Since  $\hat{R}_x$  and  $\hat{R}_z$  generate two different dissipative dynamics, two distinct engineered environments must be implemented to simulate a Markovian environment: one engineered environment to realize  $\hat{R}_x$  and the other for  $\hat{R}_z$ . Details on how this model can be implemented in a (commercial) superconducting quantum processor can be found in Ref. [22].

The total system-detector-environment dynamics is described by the operator  $\hat{U}_{\text{diss}} = \hat{u}_{\mathcal{T}} \hat{R}_z \hat{U}_z \hat{R}_x \hat{U}_x \hat{u}_1$ . In other terms, first, we couple the system and the detector to measure the system energy at the initial time. Then, we let the system evolve with  $\hat{U}_x$ , and we implement the dissipative dynamics over the  $\hat{\sigma}_x$  basis. Afterwards, the last sequence of operations is applied by changing the basis from  $x$  to  $z$ . As we are considering a QNDM scheme, after the whole evolution, we measure the phase accumulated by the detector, and we repeat the procedure by using different couplings  $\lambda$  in order to obtain the quasi-characteristic function  $\mathcal{G}_\lambda$ . Finally, the inverse Fourier transform is calculated to achieve the quasi-probability density function  $\mathcal{P}_{\text{QNDM}}(\Delta)$ .

The results from implementing this procedure in an IBM quantum processor are presented in Fig. 5. The solid curve presents the inverse Fourier transform of the experimental data; the blue dots and the red triangles are the QNDM and TPM predictions, respectively. The experimental distribution  $\mathcal{P}_{\text{QNDM}}(\Delta)$  is normalized in order to be compared with the theoretical predictions. As we can see from the figure, the experimental data and theory are in perfect agreement.

From Fig. 5, it is clear that, when there is no environment, i.e.,  $p = 0$  (panel on the left),  $\mathcal{P}_{\text{QNDM}}(\Delta)$  shows negative regions for the energy exchange of  $\varepsilon/2$  that is a forbidden transition for the TPM scheme (red dots). When the strength of the environment is increased to  $p = 0.5$ , the negative regions of  $\mathcal{P}_{\text{QNDM}}(\Delta)$  are reduced, as well as the corresponding quantum transition amplitudes; eventually, they vanish when  $p = 1$ . This trend is a signature that the interaction with the environment destroys quantum features of the dynamics, and, thus, it can be interpreted as a quantum-to-classical transition induced by the environment.

## VII. CONCLUSIONS

In this paper, we have reviewed the recent progress in interpreting and utilizing quantum non-demolition measurements to certify a violation of the macrorealism, specifically in relation to the presence of quantum interferences and coherent superpositions in the state of the quantum system under scrutiny.

The QNDM approach has two main advantages with respect to other protocols and tools present in the literature, such as LGIs [5, 27, 28, 30]. First, they give a necessary and sufficient condition for the macrorealism violation, which is directly linked with an operational procedure, discussed in Sec. IV C. By applying such a procedure, indeed, one is certain to identify — if present — the presence of quantum coherence in the quantum system state. Second, the implementation of QNDM has been already successfully carried out in several experimental laboratories worldwide, as one can evince from Refs. [22, 23, 81–84]. For these reasons, we believe that the approach based on QNDM is a privileged tool to identify quantum features of a system.

To support this claim, in this review paper, we have presented pedagogically key applications of QNDM in different physical scenarios. As the first application, we have surveyed how the QNDM can be exploited to measure the statistics of the work done by a driven quantum system without destroying the quantum interference patterns induced by the work protocol during the system dynamics. Secondly, we have shown that QNDM can be used as a tool to track the quantum-to-classical transition that a quantum system interacting with an external environment may be forced to undergo. Finally, we have discussed which is the amount of resources that are needed for the implementation of QNDM. It turns out that the number of experimental repetitions that one has to perform in order to obtain the results predicted by the QNDM approach can be greatly reduced through optimization, without losing significant information about the presence of quantum coherence.

### A. What's Next?

Given the above premises, it is clear that QNDM scheme has numerous applications in various fields of research, ranging from the foundation of quantum mechanics to quantum information and quantumness certifications. However, many studies still need to be undertaken. Below, we list some possible research directions or open points.

- Identification of a quantitative relation between the negativity of the QNDM quasi-probability distribution and a measure of quantum coherence for the current state of the measured system. The starting point would be Refs. [22, 23, 26]. Then, similar ideas might be extended to a measure of entanglement, in relation to local tests of Bell's inequalities [18].
- Detection of the quantum-to-classical transition, using the QNDM approach, for a quantum system approaching mesoscopic and even macroscopic scales. One of the open questions in the foundations of quantum mechanics, indeed, is to understand when a massive quantum body loses its quantum features, thus starting to behave classically. This line of research is still under investigation, as proved by Refs. [98–101]. In particular, in the years, double-slit experiments have been performed using different bodies with an increasing mass. Since the QNDM tracks quantum interferences and coherent superpositions, it is worth testing experimentally possible violations of macrorealism, according to QNDM quasiprobabilities, in levitated mechanical systems of mesoscopic size, as in Ref. [101].
- Application of QNDM to quantum computational complexity. In the field of quantum computing, one of the most important open questions is which fundamental resources enable a quantum advantage to be achieved. Several studies suggest that entanglement [102], nonstabilizerness [103], and quantum coherence [104, 105] are all fundamental. Recently, Thomas *et al.* [106] have shown that the “path coherence”, i.e., the interference of different paths developed during a quantum computation, is a fundamental measure to estimate the hardness of the computation and, thus, the impossibility to perform such a calculation with a classical computer. The measurement to achieve such “path coherence” might be directly related to the quasi-probability density function that arises from the QNDM protocol. While the results in Ref. [106] are exclusively theoretical, QNDM could be used to experimentally measure “path coherence” in quantum computers.

- The most used quasi-probability so far is the Wigner function (WF) [107]. As for QNDM quasi-probabilities, negative regions of the WF are used as a witness of quantum phenomena. Thus, it will be important to explore the connection between these two families of quasi-probabilities. Such a link could lead to new insights about the negativity of the WF.
- Computation of quantum speed limit bound for non-demolition quasiprobabilities, taking inspiration from Ref. [108] that addresses this issue for Kirkwood-Dirac quasiprobabilities.
- Extension of the proof of the sufficient and necessary condition for the violation of macrorealism to open quantum systems. In this regard, by setting ourselves in a context of monitoring heat generation, one could certify the presence of quantum contributions in the heat distribution using QNDM quasi-probabilities.

## ACKNOWLEDGMENTS

S.G. acknowledges financial support from the PNRR MUR project PE0000023-NQSTI funded by the European Union—Next Generation EU, and from the PRIN project 2022FEXLYB Quantum Reservoir Computing (QuReCo).

- 
- [1] J. S. Bell, *Physics Physique Fizika* **1**, 195 (1964), URL <https://link.aps.org/doi/10.1103/PhysicsPhysiqueFizika.1.195>.
- [2] S. J. Freedman and J. F. Clauser, *Phys. Rev. Lett.* **28**, 938 (1972), URL <https://link.aps.org/doi/10.1103/PhysRevLett.28.938>.
- [3] A. Aspect, P. Grangier, and G. Roger, *Phys. Rev. Lett.* **49**, 91 (1982), URL <https://link.aps.org/doi/10.1103/PhysRevLett.49.91>.
- [4] J.-W. Pan, D. Bouwmeester, H. Weinfurter, and A. Zeilinger, *Phys. Rev. Lett.* **80**, 3891 (1998), URL <https://link.aps.org/doi/10.1103/PhysRevLett.80.3891>.
- [5] A. J. Leggett and A. Garg, *Phys. Rev. Lett.* **54**, 857 (1985).
- [6] J. J. Halliwell, *Phys. Rev. A* **93**, 022123 (2016), URL <https://link.aps.org/doi/10.1103/PhysRevA.93.022123>.
- [7] J. Kofler and C. Brukner, *Phys. Rev. Lett.* **101**, 090403 (2008), URL <https://link.aps.org/doi/10.1103/PhysRevLett.101.090403>.
- [8] T. Fritz, *New Journal of Physics* **12**, 083055 (2010), URL <https://dx.doi.org/10.1088/1367-2630/12/8/083055>.
- [9] J. Kofler and i. c. v. Brukner, *Phys. Rev. A* **87**, 052115 (2013), URL <https://link.aps.org/doi/10.1103/PhysRevA.87.052115>.
- [10] C. Emary, N. Lambert, and F. Nori, *Reports on Progress in Physics* **77**, 016001 (2013), URL <https://dx.doi.org/10.1088/0034-4885/77/1/016001>.
- [11] K. S. Thorne, R. W. P. Drever, C. M. Caves, M. Zimmermann, and V. D. Sandberg, *Phys. Rev. Lett.* **40**, 667 (1978), URL <https://link.aps.org/doi/10.1103/PhysRevLett.40.667>.
- [12] V. B. Braginsky, Y. I. Vorontsov, and K. S. Thorne, *Science* **209**, 547 (1980), <https://www.science.org/doi/pdf/10.1126/science.209.4456.547>, URL <https://www.science.org/doi/abs/10.1126/science.209.4456.547>.
- [13] V. B. Braginsky, F. Y. Khalili, and K. S. Thorne, *Quantum measurement* (Cambridge University Press, Cambridge [England] ;, 1992), ISBN 052141928X.
- [14] C. M. Caves, *Phys. Rev. Lett.* **45**, 75 (1980), URL <https://link.aps.org/doi/10.1103/PhysRevLett.45.75>.
- [15] C. M. Caves, K. S. Thorne, R. W. P. Drever, V. D. Sandberg, and M. Zimmermann, *Rev. Mod. Phys.* **52**, 341 (1980), URL <https://link.aps.org/doi/10.1103/RevModPhys.52.341>.
- [16] R. Onofrio and T. Calarco, *Physics Letters A* **208**, 40 (1995), ISSN 0375-9601, URL <https://www.sciencedirect.com/science/article/pii/037596019500762R>.
- [17] T. Calarco and R. Onofrio, *Physics Letters A* **198**, 279 (1995), ISSN 0375-9601, URL <https://www.sciencedirect.com/science/article/pii/037596019401020U>.
- [18] T. Calarco and R. Onofrio, *Applied Physics B* **64**, 141 (1997), URL <https://doi.org/10.1007/s003400050158>.
- [19] P. Solinas, D. V. Averin, and J. P. Pekola, *Phys. Rev. B* **87**, 060508 (2013), URL <http://link.aps.org/doi/10.1103/PhysRevB.87.060508>.
- [20] P. Solinas and S. Gasparinetti, *Phys. Rev. E* **92**, 042150 (2015), URL <http://link.aps.org/doi/10.1103/PhysRevE.92.042150>.
- [21] P. Solinas and S. Gasparinetti, *Phys. Rev. A* **94**, 052103 (2016), URL <https://link.aps.org/doi/10.1103/PhysRevA.94.052103>.
- [22] P. Solinas, M. Amico, and N. Zanghì, *Phys. Rev. A* **103**, L060202 (2021), URL <https://link.aps.org/doi/10.1103/PhysRevA.103.L060202>.
- [23] P. Solinas, M. Amico, and N. Zanghì, *Phys. Rev. A* **105**, 032606 (2022), URL <https://link.aps.org/doi/10.1103/PhysRevA.105.032606>.
- [24] G. De Chiara, P. Solinas, F. Cerisola, and A. J. Roncaglia, *Ancilla-Assisted Measurement of Quantum Work* (Springer International Publishing, Cham, 2018), pp. 337–362, ISBN 978-3-319-99046-0, URL [https://doi.org/10.1007/978-3-319-99046-0\\_14](https://doi.org/10.1007/978-3-319-99046-0_14).
- [25] S. Gherardini and G. De Chiara, *PRX Quantum* **5**, 030201 (2024), URL <https://link.aps.org/doi/10.1103/PRXQuantum.5.030201>.

- [26] P. Solinas and S. Gherardini, Phys. Rev. A **111**, 052217 (2025), URL <https://link.aps.org/doi/10.1103/PhysRevA.111.052217>.
- [27] L. Clemente and J. Kofler, Phys. Rev. A **91**, 062103 (2015), URL <https://link.aps.org/doi/10.1103/PhysRevA.91.062103>.
- [28] L. Clemente and J. Kofler, Phys. Rev. Lett. **116**, 150401 (2016), URL <https://link.aps.org/doi/10.1103/PhysRevLett.116.150401>.
- [29] J. J. Halliwell, Phys. Rev. A **96**, 012121 (2017), URL <https://link.aps.org/doi/10.1103/PhysRevA.96.012121>.
- [30] J. J. Halliwell, J. Phys.: Conf. Ser. **1275**, 012008 (2019), URL <https://iopscience.iop.org/article/10.1088/1742-6596/1275/1/012008>.
- [31] P. Solinas, H. J. D. Miller, and J. Anders, Phys. Rev. A **96**, 052115 (2017), URL <https://link.aps.org/doi/10.1103/PhysRevA.96.052115>.
- [32] A. E. Allahverdyan, Phys. Rev. E **90**, 032137 (2014), URL <http://link.aps.org/doi/10.1103/PhysRevE.90.032137>.
- [33] S. Deffner, J. P. Paz, and W. H. Zurek, Phys. Rev. E **94**, 010103 (2016), URL <http://link.aps.org/doi/10.1103/PhysRevE.94.010103>.
- [34] F. Cerisola, Y. Margalit, S. Machluf, A. J. Roncaglia, J. P. Paz, and R. Folman, Nature Communications **8**, 1241 (2017), URL <https://www.nature.com/articles/s41467-017-01308-7>.
- [35] A. J. Roncaglia, F. Cerisola, and J. P. Paz, Phys. Rev. Lett. **113**, 250601 (2014), URL <http://link.aps.org/doi/10.1103/PhysRevLett.113.250601>.
- [36] P. Talkner, E. Lutz, and P. Hänggi, Phys. Rev. E **75**, 050102 (2007), URL <http://link.aps.org/doi/10.1103/PhysRevE.75.050102>.
- [37] A. Engel and R. Nolte, EPL (Europhysics Letters) **79**, 10003 (2007).
- [38] M. Esposito, U. Harbola, and S. Mukamel, Rev. Mod. Phys. **81**, 1665 (2009), URL <http://link.aps.org/doi/10.1103/RevModPhys.81.1665>.
- [39] M. Esposito, U. Harbola, and S. Mukamel, Rev. Mod. Phys. **86**, 1125 (2014), URL <http://link.aps.org/doi/10.1103/RevModPhys.86.1125>.
- [40] M. Campisi, P. Talkner, and P. Hänggi, Phys. Rev. Lett. **102**, 210401 (2009), URL <http://link.aps.org/doi/10.1103/PhysRevLett.102.210401>.
- [41] M. Campisi, P. Hänggi, and P. Talkner, Rev. Mod. Phys. **83**, 1653 (2011), URL <http://link.aps.org/doi/10.1103/RevModPhys.83.1653>.
- [42] D. Kafri and S. Deffner, Phys. Rev. A **86**, 044302 (2012), URL <https://link.aps.org/doi/10.1103/PhysRevA.86.044302>.
- [43] S. Hernández-Gómez, S. Gherardini, F. Poggiali, F. S. Cataliotti, A. Trombettoni, P. Cappellaro, and N. Fabbri, Phys. Rev. Res. **2**, 023327 (2020), URL <https://link.aps.org/doi/10.1103/PhysRevResearch.2.023327>.
- [44] S. Gherardini, L. Buffoni, G. Giachetti, A. Trombettoni, and S. Ruffo, Chaos, Solitons & Fractals **156**, 111890 (2022), URL <https://www.sciencedirect.com/science/article/pii/S0960077922001011>.
- [45] S. Hernández-Gómez, F. Poggiali, P. Cappellaro, F. S. Cataliotti, A. Trombettoni, N. Fabbri, and S. Gherardini, Phys. Rev. E **111**, 014139 (2025), URL <https://link.aps.org/doi/10.1103/PhysRevE.111.014139>.
- [46] R. P. Feynman and A. R. Hibbs, *Quantum mechanics and path integrals* (McGraw-Hill, 1965).
- [47] M. Perarnau-Llobet, E. Bäumer, K. V. Hovhannisyann, M. Huber, and A. Acin, Phys. Rev. Lett. **118**, 070601 (2017), URL <https://link.aps.org/doi/10.1103/PhysRevLett.118.070601>.
- [48] M. Lostaglio, A. Belenchia, A. Levy, S. Hernandez-Gomez, N. Fabbri, and S. Gherardini, Quantum **7**, 1128 (2023), URL <https://quantum-journal.org/papers/q-2023-10-09-1128/>.
- [49] K. Micadei, G. T. Landi, and E. Lutz, Phys. Rev. Lett. **124**, 090602 (2020), URL <https://link.aps.org/doi/10.1103/PhysRevLett.124.090602>.
- [50] K. Micadei, J. P. S. Peterson, A. M. Souza, R. S. Sarthour, I. S. Oliveira, G. T. Landi, R. M. Serra, and E. Lutz, Phys. Rev. Lett. **127**, 180603 (2021), URL <https://link.aps.org/doi/10.1103/PhysRevLett.127.180603>.
- [51] S. Gherardini, A. Belenchia, M. Paternostro, and A. Trombettoni, Phys. Rev. A **104**, L050203 (2021), URL <https://link.aps.org/doi/10.1103/PhysRevA.104.L050203>.
- [52] S. Hernández-Gómez, S. Gherardini, A. Belenchia, A. Trombettoni, M. Paternostro, and N. Fabbri, npj Quantum Information **9**, 86 (2023), URL <https://doi.org/10.1038/s41534-023-00738-0>.
- [53] I. Gianani, A. Belenchia, S. Gherardini, V. Berardi, M. Barbieri, and M. Paternostro, Quantum Sci. Technol. **8**, 045018 (2023), URL <https://iopscience.iop.org/article/10.1088/2058-9565/acedca>.
- [54] A. Sone, Y.-X. Liu, and P. Cappellaro, Phys. Rev. Lett. **125**, 060602 (2020), URL <https://link.aps.org/doi/10.1103/PhysRevLett.125.060602>.
- [55] A. Bednorz and W. Belzig, Phys. Rev. Lett. **105**, 106803 (2010), URL <http://link.aps.org/doi/10.1103/PhysRevLett.105.106803>.
- [56] G. Bizzarri, S. Gherardini, M. Manrique, F. Bruni, I. Gianani, and M. Barbieri, Quantum Sci. Technol. **10**, 045008 (2025), URL <https://iopscience.iop.org/article/10.1088/2058-9565/adf573>.
- [57] P. P. Hofer and A. A. Clerk, Phys. Rev. Lett. **116**, 013603 (2016), URL <http://link.aps.org/doi/10.1103/PhysRevLett.116.013603>.
- [58] M. Lostaglio, Phys. Rev. Lett. **120**, 040602 (2018), URL <https://link.aps.org/doi/10.1103/PhysRevLett.120.040602>.
- [59] P. P. Potts, Phys. Rev. Lett. **122**, 110401 (2019), URL <https://link.aps.org/doi/10.1103/PhysRevLett.122.110401>.
- [60] A. Levy and M. Lostaglio, PRX Quantum **1**, 010309 (2020), URL <https://link.aps.org/doi/10.1103/PRXQuantum.1.010309>.
- [61] S. Hernández-Gómez, S. Gherardini, A. Belenchia, M. Lostaglio, A. Levy, and N. Fabbri, Phys. Rev. Res. **6**, 023280 (2024), URL <https://link.aps.org/doi/10.1103/PhysRevResearch.6.023280>.

- [62] S. Hernández-Gómez, T. Isogawa, A. Belenchia, A. Levy, N. Fabbri, S. Gherardini, and P. Cappellaro, *npj Quantum Information* **10** (2024), URL <https://www.nature.com/articles/s41534-024-00913-x>.
- [63] D. R. M. Arvidsson-Shukur, W. F. Braasch Jr., S. De Bievre, J. Dressel, A. N. Jordan, C. Langrenez, M. Lostaglio, J. S. Lundeen, and N. Yunger Halpern, *New J. Phys.* **26**, 121201 (2024), URL <https://iopscience.iop.org/article/10.1088/1367-2630/ada05d>.
- [64] T. Upadhyaya, W. F. Braasch, G. T. Landi, and N. Y. Halpern, *PRX Quantum* **5**, 030355 (2024), URL <https://link.aps.org/doi/10.1103/PRXQuantum.5.030355>.
- [65] M. Pezzutto, G. De Chiara, and S. Gherardini, *Quantum Sci. Technol.* **10**, 035066 (2025), URL <https://iopscience.iop.org/article/10.1088/2058-9565/aded2e>.
- [66] R. Dorner, S. R. Clark, L. Heaney, R. Fazio, J. Goold, and V. Vedral, *Phys. Rev. Lett.* **110**, 230601 (2013), URL <http://link.aps.org/doi/10.1103/PhysRevLett.110.230601>.
- [67] L. Mazzola, G. De Chiara, and M. Paternostro, *Phys. Rev. Lett.* **110**, 230602 (2013), URL <http://link.aps.org/doi/10.1103/PhysRevLett.110.230602>.
- [68] F. Petruccione and H.-P. Breuer, *The theory of open quantum systems* (Oxford Univ. Press, 2002).
- [69] M. Campisi, P. Hänggi, and P. Talkner, *Rev. Mod. Phys.* **83**, 771 (2011), URL <http://link.aps.org/doi/10.1103/RevModPhys.83.771>.
- [70] K. Blum, *Density matrix theory and applications*, Springer series on atomic, optical, and plasma physics (Springer, Berlin, 2012), URL <https://cds.cern.ch/record/1433745>.
- [71] J. Pekola, P. Solinas, A. Shnirman, and D. Averin, *New Journal of Physics* **15**, 115006 (2013).
- [72] S. Gasparinetti, K. L. Viisanen, O.-P. Saira, T. Faivre, M. Arzeo, M. Meschke, and J. P. Pekola, *Phys. Rev. Applied* **3**, 014007 (2015), URL <https://link.aps.org/doi/10.1103/PhysRevApplied.3.014007>.
- [73] K. L. Viisanen, S. Suomela, S. Gasparinetti, O.-P. Saira, J. Ankerhold, and J. P. Pekola, *New Journal of Physics* **17**, 055014 (2015), URL <https://doi.org/10.1088/2F1367-2630/2F17/2F5/2F055014>.
- [74] O.-P. Saira, M. Zgirski, K. L. Viisanen, D. S. Golubev, and J. P. Pekola, *Phys. Rev. Applied* **6**, 024005 (2016), URL <https://link.aps.org/doi/10.1103/PhysRevApplied.6.024005>.
- [75] V. Vesterinen, O.-P. Saira, I. Räisänen, M. Möttönen, L. Grönberg, J. Pekola, and J. Hassel, *Superconductor Science and Technology* **30**, 085001 (2017), URL <https://doi.org/10.1088/2F1361-6668/2Faa73ed>.
- [76] A. Ronzani, B. Karimi, J. Senior, Y.-C. Chang, J. T. Peltonen, C. Chen, and J. P. Pekola, *Nature Physics* **14**, 991 (2018), URL <https://doi.org/10.1038/s41567-018-0199-4>.
- [77] R. Alicki, *J. Phys. A: Math. Gen.* **12**, L103 (1979), URL <https://iopscience.iop.org/article/10.1088/0305-4470/12/5/007>.
- [78] O. J. E. Maroney and C. G. Timpson, arXiv preprint arXiv:1412.6139 (2014), URL <https://doi.org/10.48550/arXiv.1412.6139>.
- [79] D. Schmid, *Quantum* **8**, 1217 (2024), ISSN 2521-327X, URL <https://doi.org/10.22331/q-2024-01-03-1217>.
- [80] G. C. Knee, K. Kakuyanagi, M.-C. Yeh, Y. Matsuzaki, H. Toida, H. Yamaguchi, S. Saito, A. J. Leggett, and W. J. Munro, *Nature Communications* **7**, 13253 (2016), URL <https://doi.org/10.1038/ncomms13253>.
- [81] J. Geremia, J. K. Stockton, A. C. Doherty, and H. Mabuchi, *Phys. Rev. Lett.* **91**, 250801 (2003), URL <https://link.aps.org/doi/10.1103/PhysRevLett.91.250801>.
- [82] C. Guerlin, J. Bernu, S. Deléglise, C. Sayrin, S. Gleyzes, S. Kuhr, M. Brune, J.-M. Raimond, and S. Haroche, *Nature* **448**, 889 (2007), URL <https://www.nature.com/articles/nature06057>.
- [83] D. Niemietz, P. Farrera, S. Langenfeld, and G. Rempe, *Nature* **591**, 570 (2021), URL <https://www.nature.com/articles/s41586-021-03290-z>.
- [84] R. Yanagimoto, R. Nehra, R. Hamerly, E. Ng, A. Marandi, and H. Mabuchi, *PRX Quantum* **4**, 010333 (2023), URL <https://link.aps.org/doi/10.1103/PRXQuantum.4.010333>.
- [85] L. S. Levitov and G. B. Lesovik, *Pis'ma Zh. Eksp. Teor. Fiz. [JETP Lett.]* **58**, 230 (1993).
- [86] L. S. Levitov, H. Lee, and G. B. Lesovik, *J. Math. Phys.* **37**, 4845 (1996), URL <https://doi.org/10.1063/1.531672>.
- [87] Y. V. Nazarov and M. Kindermann, *Eur. Phys. J. B* **35**, 413 (2003), URL <http://dx.doi.org/10.1140/epjb/e2003-00293-1>.
- [88] A. A. Clerk, *Phys. Rev. A* **84**, 043824 (2011), URL <http://link.aps.org/doi/10.1103/PhysRevA.84.043824>.
- [89] A. Bednorz, W. Belzig, and A. Nitzan, *New J. Phys.* **14**, 013009 (2012), URL <http://stacks.iop.org/1367-2630/14/i=1/a=013009>.
- [90] W. Belzig and Y. V. Nazarov, *Phys. Rev. Lett.* **87**, 197006 (2001), URL <http://link.aps.org/doi/10.1103/PhysRevLett.87.197006>.
- [91] B. Reulet, A. A. Kozhevnikov, D. E. Prober, W. Belzig, and Y. V. Nazarov, *Phys. Rev. Lett.* **90**, 066601 (2003), URL <https://link.aps.org/doi/10.1103/PhysRevLett.90.066601>.
- [92] A. V. Timofeev, M. Meschke, J. T. Peltonen, T. T. Heikkilä, and J. P. Pekola, *Phys. Rev. Lett.* **98**, 207001 (2007), URL <https://link.aps.org/doi/10.1103/PhysRevLett.98.207001>.
- [93] V. F. Maisi, D. Kambly, C. Flindt, and J. P. Pekola, *Phys. Rev. Lett.* **112**, 036801 (2014), URL <https://link.aps.org/doi/10.1103/PhysRevLett.112.036801>.
- [94] D. Melegari, M. Cardi, and P. Solinas, *Phys. Rev. A* **111**, 052435 (2025), URL <https://link.aps.org/doi/10.1103/PhysRevA.111.052435>.
- [95] A. Javadi-Abhari, M. Treinish, K. Krsulich, C. J. Wood, J. Lishman, J. Gacon, S. Martiel, P. D. Nation, L. S. Bishop, A. W. Cross, et al., arXiv preprint arXiv:2405.08810 (2024), URL <https://doi.org/10.48550/arXiv.2405.08810>.
- [96] M. A. Nielsen and I. L. Chuang, *Quantum computation and quantum information* (Cambridge University Press, Cambridge, UK, 2010).
- [97] G. García-Pérez, M. A. C. Rossi, and S. Maniscalco, *npj Quantum Information* **6**, 1 (2020), URL <https://doi.org/10.1038/s41534-019-0235-y>.

- [98] M. Arndt, O. Nairz, J. Vos-Andreae, C. Keller, G. van der Zouw, and A. Zeilinger, *Nature* **401**, 680 (1999), URL <https://doi.org/10.1038/44348>.
- [99] S. Gerlich, S. Eibenberger, M. Tomandl, S. Nimmrichter, K. Hornberger, P. J. Fagan, J. Tüxen, M. Mayor, and M. Arndt, *Nature Communications* **2**, 263 (2011), URL <https://doi.org/10.1038/ncomms1263>.
- [100] M. Aspelmeyer, *When Zeh Meets Feynman: How to Avoid the Appearance of a Classical World in Gravity Experiments* (Springer International Publishing, Cham, 2022), pp. 85–95, ISBN 978-3-030-88781-0, URL [https://doi.org/10.1007/978-3-030-88781-0\\_5](https://doi.org/10.1007/978-3-030-88781-0_5).
- [101] T. M. Fuchs, D. G. Uitenbroek, J. Plugge, N. van Halteren, J.-P. van Soest, A. Vinante, H. Ulbricht, and T. H. Oosterkamp, *Science Advances* **10**, 1 (2024), URL <https://doi.org/10.1126/sciadv.adk2949>.
- [102] R. Horodecki, P. Horodecki, M. Horodecki, and K. Horodecki, *Rev. Mod. Phys.* **81**, 865 (2009), URL <https://link.aps.org/doi/10.1103/RevModPhys.81.865>.
- [103] L. Leone, S. F. E. Oliviero, and A. Hamma, *Phys. Rev. Lett.* **128**, 050402 (2022), URL <https://link.aps.org/doi/10.1103/PhysRevLett.128.050402>.
- [104] T. Baumgratz, M. Cramer, and M. B. Plenio, *Phys. Rev. Lett.* **113**, 140401 (2014), URL <https://link.aps.org/doi/10.1103/PhysRevLett.113.140401>.
- [105] A. Streltsov, G. Adesso, and M. B. Plenio, *Rev. Mod. Phys.* **89**, 041003 (2017), URL <https://link.aps.org/doi/10.1103/RevModPhys.89.041003>.
- [106] H. Thomas, P.-E. Emeriau, R. Mezher, E. Kashefi, H. Ollivier, and U. Chabaud, *Phys. Rev. Lett.* **135**, 150602 (2025), URL <https://link.aps.org/doi/10.1103/1csn-x1cx>.
- [107] M. Hillery, R. O’Connell, M. Scully, and E. Wigner, *Physics Reports* **106**, 121 (1984), ISSN 0370-1573, URL <https://www.sciencedirect.com/science/article/pii/0370157384901601>.
- [108] S. S. Pratapsi, S. Deffner, and S. Gherardini, *Quantum Sci. Technol.* **10**, 035019 (2025), URL <https://iopscience.iop.org/article/10.1088/2058-9565/add55d>.